A model for archaeologically relevant Holocene climate impacts in the Aegean-Levantine region (easternmost Mediterranean)

Eelco J. Rohling[1,2], Gianluca Marino[1,3], Katharine M. Grant[1], Paul A. Mayewski[4], and Bernhard Weninger[5]

1. Research School of Earth Sciences, The Australian National University, Canberra, ACT, 2601, Australia.
2. Ocean and Earth Science, University of Southampton, National Oceanography Centre, Southampton SO14 3ZH, UK.
3. Department of Marine Geosciences and Territorial Planning, University of Vigo, 36310 Vigo, Spain.
4. Climate Change Institute, University of Maine, Orono, USA.
5. Institut für Ur- und Frühgeschichte, Universität zu Köln, Weyertal 125, D-50931 Köln, Germany.

Abstract. A repeating pattern of multi-centennial-scale Holocene climate events has been widely (globally) documented, and they were termed Rapid Climate Change (RCC) events. Non-seasalt potassium ion (K^+) series in Greenland ice cores provide well-constrained timings for the events, and a direct timing relationship has been inferred between these events and the frequency of northerly cold polar/continental air outbreaks over the eastern Mediterranean Sea through gaps in the mountain ranges along the northern margin of the basin. There also appears to be a remarkable timing agreement with major archaeological turnover events in the Aegean/Levantine region. Yet no physically consistent assessment exists for understanding the regional climatic impacts of the events around this critical region. We present a simple 2-dimensional Lagrangian model, which yields a broad suite of physically coherent simulations of the impacts of frequency changes in winter-time northerly air outbreaks over the Aegean/Levantine region. We validate this with existing reconstructions from palaeoclimate proxy data, with emphasis on well-validated sea-surface temperature reconstructions and a highly resolved cave speleothem stable oxygen isotope record from Lebanon. Given that the RCCs were clearly marked by negative sea surface temperature anomalies in the region, we find that the predominant climatic impacts of this winter-time mechanism were "cold and wet," in contrast with intercalated "warmer and more arid" conditions of non-RCC periods. More specifically, the RCCs are found to be periods of highly variable conditions, with an overall tendency toward cold and wet conditions with potential for flash flooding and for episodic snow-cover at low altitudes, at least in the lower-altitude (lower 1 to 1.5 km) regions of Crete and the Levant. The modelled winter-anomaly process cannot address underlying longer-term, astronomically forced trends, or the relatively warm and arid anomalies in between RCCs. The latter require further study, for example with respect to potential (summer-time?) extension of evaporative subtropical conditions over the region. Finally, our results imply that the "amount effect" observed in Levantine cave $\delta^{18}O$ (and precipitation or drip-water $\delta^{18}O$) may not reflect the conventional concept related to temperature-dependent fractionation and Rayleigh distillation. Instead, it appears to arise from a complex and somewhat counter-intuitive mixing, in shifting proportionalities, between advected (external) and evaporated (Mediterranean) moisture.

1. INTRODUCTION

A series of globally widespread climate anomalies occurred during the Holocene, namely the Holocene "Rapid Climate Change" events (RCCs), focussed on 9-8 ka BP, 6-5 ka BP, 4.2-3.8 ka BP, 3.5-2.5 ka BP, 1.2-1.0 ka BP, and 0.6-0.15 ka BP (the Little Ice Age; LIA) (Mayewski et al., 2004 and references therein). These events, dated with the precise Greenland ice-core chronologies, were characterised by chemical signatures in Greenland ice cores, notably non-seasalt (nss) K^+ increases, which have been correlated to intensified Siberian High (pressure) conditions in winter/early spring (Mayewski et al., 1997; Meeker and Mayewski, 2002; O'Brien et al., 1995). The very brief 4.2-3.8 ka BP and 1.2-1.0 ka BP events form exceptions to this relationship with $nssK^+$ increases, and thus seem to be different from the other, longer events. Note that all ages discussed in this paper are calibrated ages referenced as Before Present, where Present is the year 1950.

The main RCCs are distinctly expressed in the eastern Mediterranean Sea, showing up as ~2 °C (up to 3 °C) "cold spells" in Aegean and Adriatic sea surface temperature (SST) records at 8.6-8.0 (or 7.8) ka BP, 6-5.2 ka BP, 3.1-2.9 ka BP, and the LIA (Rohling et al., 1997; Casford et al., 2001, 2003; Mercone et al., 2001; Rohling et al., 2002a,b, 2009; Clare et al., 2008; Marino et al., 2009; Clare, 2016; Gogou et al., 2016). Given the vast heat capacity of water relative to overlying air, such multi-centennial (long-term) mean cooling of the ~100 m thick surface mixed layer implies intense atmospheric forcing. This inference is further strengthened by deep-water data, from the same samples as the surface-cooling data, which suggest that even deep-water circulation was affected (intensified) at these times (Rohling et al., 1997; Rohling et al., 2002a; Kuhnt et al., 2007; Abu-Zied et al., 2008; Schmiedl et al., 2010).

Previous work (e.g., Rohling et al., 2002b; Casford et al., 2003; Clare et al., 2008; Weninger et al., 2009, 2014) has sought to relate the distinct eastern Mediterranean RCC signals to processes that involve the Siberian High intensifications indicated by consistent Greenland ice-core $nssK^+$ enrichments (O'Brien et al., 1995; Mayewski et al., 2004; Muschitiello et al., 2013), but debate remains about the underlying atmospheric dynamics (*see section 2.1*). In any case, the critical component for the eastern Mediterranean was found to consist of increases in the frequency and/or intensity of cold northerly polar/continental (NPC) air outbreaks over the sea that are channelled through gaps in the mountain ranges along the basin's northern margin (*section 2.1*). So far, no physically consistent assessments exist for the regional climatic impacts of the RCCs, despite the fact that understanding of these events is of central importance for studies concerning vulnerability and response of prehistoric societies to climate and environmental change in the wider Mediterranean region (e.g., Anderson et al., 2007; Biehl and Nieuwenhuyse, 2016; Budja, 2007, 2015; Weiberg et al., 2016; Weiss, 2000; 2017) (*section 2.4*).

This study first reviews modern and past expressions of wintertime cold polar/continental air outbreaks from the north over the Aegean Sea, and then develops a physically coherent 2-dimensional Lagrangian assessment of the inferred RCC relationships over the Aegean/eastern Levantine region. This assessment is used to quantify the expected signals of the processes involved, and finally the expected signals are compared with palaeoclimatological records through the Holocene RCC intervals.

2. BACKGROUND

2.1. Instrumentally documented events

Individual wintertime NPC air outbreaks from higher latitudes over the Aegean Sea and into the Levantine region have been well documented during the instrumental era (Mariolopoulos, 1961; Theocharis, 1989; Roether et al., 1996; Poulos et al., 1997; Maheras et al., 1999; Lolis et al., 2002; Tolika et al., 2014; Anagnostopoulou et al., 2017). No NPC air outbreaks occur during the summer months (Saaroni et al., 1996). In winter, North African subtropical conditions are displaced southward (Lionello et al., 2006; Rohling et al., 2015), allowing a general southward expansion of westerly, moist temperate airflows, as well as occasional atmospheric blocking patterns that drive cold and dry polar/continental air outbreaks from the North (e.g., Tolika et al., 2014). Over the central and eastern Mediterranean Sea, low surface-pressure conditions persist even during these outbreaks because the sea's high thermal capacity maintains a contrast between relatively high sea-surface temperatures and the colder surrounding landmasses (Lolis et al., 2002).

The main drivers for winter-time heat loss from the Mediterranean are the so-called "East Atlantic" and "East Atlantic/West Russian" (EA and EA/WR) atmospheric circulation modes (Josey et al., 2011), when Mediterranean low-pressure conditions interact with a north-eastward extension of the Azores High (over Iberia, France, and southern Britain), and/or westward ridging of the Siberian High towards North-West Europe and southern Scandinavia (Maheras et al., 1999; Lolis et al., 2002; Tolika et al., 2014). During the EA or EA/WR modes, intense northerly flows of cold and dry air masses toward the Mediterranean basin are channelled through valleys in the mountainous topography of the basin's northern margin. In the eastern Mediterranean, channelling occurs through river valleys—such as that of the Axios (Vardar zone), Strimon, and Evros—towards the Adriatic and Aegean Seas, where it gives rise to the "Bora" and "Vardar" winds, respectively.

The atmospheric dynamical configurations that underpin persistent Aegean cooling events over decadal to centennial scales remain subject to debate. They have been ascribed to a number of patterns. The first invokes frequent protrusion of a polar trough into the Mediterranean region, favoured by northward extension of the Azores High toward Iceland or Greenland—blocking moisture supply by the westerlies—and further enhanced by expansion and intensification of the Siberian High in winter during glacial times (Kuhlemann et al., 2008). Luterbacher et al. (2006) find that the most important Mediterranean cold pattern corresponds to a blocking configuration with easterly to northeasterly airflow towards the Mediterranean, and that cooler and wetter conditions in the last decades of the seventeenth century coincided with and increase in the surface Russian High pressure influence, which caused easterly dry and cold airflow to advance further to the west, The second pattern involves a multicentennial reduction in the northward heat transport by the North Atlantic subpolar gyre, with internal climate feedbacks—notably increases in Scandinavian blocking event frequency—causing winter amplification of the European Little Ice Age cooling (Moreno-Chamarro et al., 2017). The third suggested pattern concerns a positive state of the EA/WR pattern that results in strongly enhanced heat loss over the Aegean region (Josey et al., 2011), combined with positive North Atlantic Oscillation phases that lead to decreased winter precipitation, and negative Atlantic Meridional Oscillation phases that further intensify

149 cooling in the Aegean region (Incarbona et al., 2016). Tolika et al. (2014) described a
150 strong pattern for the entire, cold, winter of 2012 (hence, not just for a short event),
151 which integrates many of the individual features discussed above. They find both
152 intensification and northward extension of the Azores High, and—especially—
153 westward extension of high-pressure conditions throughout Asia (Siberian High)
154 toward the Balkans and northern Europe. Tolika et al. (2014) infer that the latter
155 caused blocking of the atmospheric circulation on its western side over Scandinavia,
156 eastern Europe, and the eastern Mediterranean, which in turn favoured transfer of cold
157 air masses from high northern latitudes over the Balkan and eastern Mediterranean.
158 Anagnostopoulou et al. (2017) noted considerable large-scale similarities during a cold
159 event in winter 2017. In context of the above, we view the Siberian High not as a unique
160 driver, but as a correlated part (higher pressures correlating with intensified Aegean
161 cooling) of wider northern hemispheric circulation modes that enhance advection of
162 cold air from high latitudes toward the eastern Mediterranean, and which—for
163 instance—also include deepening/shoaling of a Low between Iceland and southern
164 Greenland (Panagiotopoulos et al., 2005; Tubi and Dayan, 2013).
165
166 Regardless of the precise underpinning dynamics, enhanced wintertime cold NPC air
167 outbreaks cause intense evaporation and cooling of the Mediterranean Sea surface (e.g.,
168 Leaman and Schott, 1991; Saaroni et al., 1996; Poulos et al., 1997; Maheras et al., 1999;
169 Casford et al., 2003; Josey et al., 2011; Velaoras et al., 2017). A particularly noticeable
170 period with frequent events over the Aegean occurred in the late 1980s-early 1990s,
171 contributing to profound changes in deep-water formation in the region (Theocharis,
172 1989; Roether et al., 1996). Casford et al. (2003) drew on this—along with new
173 shipboard data for a December 2001 event—to infer the impacts of prolonged episodes
174 with high event intensity/frequency on deep-water circulation in the Aegean-Levantine
175 region throughout the Holocene (for indicators of Holocene deep-water changes, see
176 Rohling et al., 2002a; Kuhnt et al., 2007; Abu-Zied et al., 2008; Schmiedl et al., 2010).
177 Incarbona et al. (2016) similarly found a relationship within the past 500 years between
178 multi-decadal deep-water ventilation changes in the eastern Mediterranean and surface
179 cooling events. Deep-water ventilation records provide the most convincing means of
180 identifying the most intense episodes of clustered events, given that climatic anomalies
181 of considerable strength and cumulative duration are needed to intensify deep-water
182 formation and deep-sea ventilation.
183
184 The environmental impacts of an individual cold NPC air outbreak are well illustrated
185 by the 2001 event (Casford et al., 2003), which lasted (with variations) from December
186 2001 to January 2002, and was marked by high-intensity (8-9 Beaufort, or 17-25 m s^{-1}),
187 freezing (down to –2°C), north-northeasterly airflow over the Aegean Sea (Casford et al.,
188 2003; Clare et al., 2008). There was exceptional snowfall around the Aegean region,
189 including ~30 cm in both Istanbul and Athens (see summary in Clare et al., 2008).
190 Temperatures in Bulgaria and northern and central-eastern Greece dropped to minima
191 of –20 °C, and there was widespread disruption of infrastructure and services (see
192 summary in Clare et al., 2008). More than 300 villages in central and northern Greece
193 became isolated, and there were many deaths from exposure (World Weather News,
194 2001; CNN Weather, 2001). In earlier years, 1929 and 1954, conditions became so
195 severe that much of the Bosporus froze over (Yavuz et al., 2007).
196

197 Finally, cold NPC air outbreaks are known to play a key role in cyclogenesis over the
198 eastern Mediterranean, and in particular the Cyprus Low, which governs a large portion
199 of rainfall over the Middle East. Tarolli et al. (2012) state that: "… *over the*
200 *Mediterranean climate areas of Israel, high precipitation events and extreme flash floods*
201 *are mainly associated with the Cyprus Low, … a winter extra-tropical cyclone … system…*
202 *(Sharon and Kutiel, 1986; Alpert et al., 1990; Krichak et al., 2004; Ziv et al., 2006;*
203 *Wittenberg et al., 2007; Saaroni et al., 2010). The cold air masses gain moisture … over*
204 *warmer Mediterranean waters and become conditionally unstable. … An upper-level*
205 *trough extending toward southwestern Turkey induces cold advection aloft, enhancing*
206 *cyclogenic conditions over the Cyprus Low region."* Overall, therefore, the cold NPC air
207 outbreaks were found to be critical drivers of downstream hydroclimate conditions
208 over the lands that border the Levantine Sea, easternmost Mediterranean, during the
209 instrumental era.
210
211 ***2.2. The Little Ice Age***
212 Assessments of terrestrial palaeoclimate proxy records around the Mediterranean that
213 pre-date the instrumental era have inferred notable hydroclimate variations, including
214 arid episodes (Roberts et al., 2011; Cheng et al., 2015; Clarke et al., 2016), and some
215 have inferred spatial hydrological contrasts (Roberts et al., 2011; Cheng et al., 2015).
216 However, comparisons between terrestrial signals, and between terrestrial and marine
217 signals, may be compromised by: 1) offsets/uncertainties between chronologies; 2)
218 comparing records of different temporal resolutions (e.g., Clarke et al., 2016); 3)
219 regionally differentiated climatic expressions (e.g., with altitude, or upstream *versus*
220 downstream relative to the evaporative sea); and/or 4) inaccurate or oversimplified
221 assumptions about processes controlling the palaeoclimate records.
222
223 One way to advance is through comparison of instrumentally documented events
224 (above) with documentary/anecdotal evidence for the Little Ice Age (LIA) to evaluate
225 the range of impacts of sustained cold NPC air outbreaks over the Aegean-Levantine
226 region (e.g., Xoplaki et al., 2001; Yavuz et al., 2007; Clare et al., 2008; Clare, 2016). This
227 reveals that instrumentally documented impacts resonate strongly with the regional
228 LIA accounts. For example, Xoplaki et al. (2001) report that the LIA was characterised
229 by: more cold/severe winters and springs; a significant tendency to more winter
230 precipitation (with notable prevalence of snow, which in the year 1700 even survived
231 through summer on the Cretan mountains); and by significantly more winter drought.
232 In short, there was a significant increase in winter extremes, being either very cold, very
233 wet/snowy, or very dry. A subsequent LIA compilation further supported this inference
234 of a significant increase in winter extremes in the eastern Mediterranean region (Clare,
235 2016). The main synoptic situations responsible for the region's winter cold and
236 snowfalls again involved northerly airflow, with high pressure over northern Europe
237 and lower pressure over the central or eastern Mediterranean (Xoplaki et al., 2001).
238
239 During the LIA, glacier development/expansion occurred in many Mediterranean
240 mountain locations, while (semi-)permanent snowfields became established in the
241 mountains of Greece, which are too dry for glacier development (Hughes, 2014). This
242 requires not only cold, but also moisture supply. In the Pirin Mountains, SW Bulgaria,
243 there even was a drop in mean summer temperatures by 2-3 °C at around 1600 AD: soil
244 formation processes came to a halt, the snowline descended, the vegetation period

became shortened, and snow cover persisted for longer (Grunewald and Scheithauer, 2010).

Between 1600 and 1930, frequent widespread freezing events affected the Black Sea, Bosporus, Golden Horn, and Istanbul region (Yavuz et al., 2007), and mean surface mixed-layer temperature dropped by ~2 °C in the northern Aegean Sea between about 1650 and 1850 (Gogou et al., 2016). In addition, flooding frequencies and fluvial discharge were increased around the Aegean (see overview in Gogou et al., 2016), although stable oxygen isotope data from the high-altitude (1363 m) central Anatolian lake Nar Göülu show a positive 2-3 ‰ LIA anomaly that has been interpreted in terms of increased aridity (Dean et al., 2013). If correct, this might reflect a remarkable spatial and/or vertical contrast, possibly due to specific local conditions for the Anatolian highlands (e.g., increased lake evaporation into high-altitude, cold, low-humidity air under high wind speeds, see also *section 5*).

2.3. Older Holocene RCCs
Similar to the LIA, other Holocene RCCs were also associated with notable environmental changes in the Aegean-Levantine region. In this section, we illustrate the main impacts across a number of mid-to-late Holocene events. Mean terrestrial coolings of more than 4 °C have been reconstructed to the north of the Mediterranean, e.g., in NW Romania (Feurdean et al., 2008), SW Romania (Poleva Cave; Constantin et al., 2007), and—at least for the 8.2 ka BP event—in northern Greece (Pross et al., 2009). As mentioned above, all main RCCs are expressed as ~2 °C (up to 3 °C) drops in Aegean and Adriatic sea surface temperatures (SST). Given this distinct SST signature, and the vast heat capacity of an ~100-m-thick mixed layer, much sharper and more pronounced terrestrial climatic impacts should be expected.

In view of the NPC air-outbreak mechanism behind the events, terrestrial impacts likely were highly variable in time, with considerable extremes (in marine records, such variability is smoothed out by both longer time-integration due to oceanic inertia, and multi-decadal smoothing in the sediments investigated). Rohling et al. (2009) speculated that, during the RCCs, intensified winter frosts and aridity might especially be expected upwind of the sea (along the northern and northeastern sectors of the Aegean), while milder but still anomalously cool conditions with exceptional snow- or rainfalls might be expected downwind of the evaporative sea, when air rises and cools during convection or orographic uplift. This seems to be supported by the findings of Valsecchi et al. (2012) that apparent forest retreat occurred during several of the RCC periods around the Sea of Marmara, in coincidence with sea-surface cooling noted in the same sediment core, suggesting a combination of cold and arid conditions in that location to the northeast of the Aegean Sea.

As an important aside, note that the RCC between 8.6 and ~8.0 or 7.8 ka BP contains within it a sharp, short-lived event (~150 years; Thomas et al., 2007), from about 8.2 ka BP. This is the so-called "8.2 ka BP" event that is widely ascribed to a final glacial meltwater outbreak into the North Atlantic from Hudson Bay (e.g., Alley et al., 1997; Barber et al., 1999). The superimposition of the 8.2 ka BP event upon a major multi-century RCC has been well documented on a (near) global scale (Rohling and Pälike, 2005), including the Aegean region (Marino et al., 2009; Schemmel et al., 2016). Care must be taken not to confuse one with the other (see also Weninger et al., 2014). Our

294   main focus here is on the recurring Holocene RCCs driven directly by changes in
295   atmospheric circulation.
296
297   Between 8.6 and 8.0 ka BP, there definitely was Aegean-Levantine cooling, along with
298   improved deep-water ventilation (e.g., Rohling et al., 2002a,b; Kuhnt et al., 2007; Abu-
299   Zied et al., 2008; Schmiedl et al., 2010), as seen in other RCC events. To the south,
300   African monsoon indicators suggest that the Blue Nile contribution into the eastern
301   Mediterranean, which had reached a peak from ~10.5 ka BP (following a gradual
302   increase that started at ~12 ka BP) started a sharp decline from ~8.4 ka BP. African
303   monsoon conditions then became unstable: input into the eastern Mediterranean
304   became more dominated by White Nile fluctuations and disappeared gradually, with
305   modern-type aridity reached at around 6 to 5.5 ka BP (cf. Revel et al., 2010; and
306   references therein). So the RCC of 8.6-8.0 ka BP was a time of remarkable change in the
307   wider study region, when centennial-scale RCC-style conditions coincided with major
308   change in the orbital-scale conditions. Interpreting archaeological responses as caused
309   by one or the other may be impossible, but focussing on the specific climatic effects
310   expected from the RCC-style overprint of this period is possible, and is attempted here.
311

312 ***2.4. Archaeological importance***
313   RCCs have been previously linked to archaeological changes, either in terms of temporal
314   coincidence, or even in terms of causality. In this section, we summarise some of these
315   indications.
316
317   A first example pertains to the initial domestication of plants and animals in the Near
318   East during the Early Holocene. Some interpret this as a slow and gradual process based
319   on cultural (millennial) timescales (e.g., Fuller et al., 2012; Asouti and Fuller, 2013), and
320   others see it as a rapid process over much shorter biological (decadal) timescales (e.g.,
321   Hillman and Davies, 1990; Honne and Heun, 2009; Heun et al., 2012). A recent
322   reanalysis (Weninger, 2017) of published archaeobotanical and archaeozoological data
323   indicates that the wild-domesticate transition (WDT) occurred (1) abruptly at around
324   10.2±0.2 ka BP, (2) simultaneously (within given error limits) for plants and animals,
325   and (3) synchronously with the abrupt onset of moist conditions in the Near East
326   (Schmiedl et al., 2010; Sharifi et al. 2015). It appears that, in terms of understanding the
327   introduction of farming and stock-breeding, past research placed too much emphasis on
328   the Younger Dryas (YD), given that the YD ended as much as 1500 years before the
329   WDT. Regardless, it remained poorly understood why the transition to agriculture
330   would have coincided (within error limits) with a sharp RCC-event at 10.23 ka BP,
331   which is very apparent in the GISP2 nss K+ record (Mayewski et al., 1997). While this
332   might be a chance coincidence, Borrell et al., (2015) reported a major cultural
333   discontinuity at around 10.2-9.8 ka BP in Neolithic communities in most of the Northern
334   Levant, which again coincides closely (within error limits) with this RCC-event. And a
335   similar time-gap also exists in the Southern Levant (e.g., at Jericho; Bar-Yosef, 1986).
336
337   For the next RCC (8.6 to ~8.0 ka BP), a previous compilation of climate indicator studies
338   throughout southeastern Europe, Anatolia, Cyprus, and the Near East was taken to
339   suggest 'cold and arid' conditions at around 8.2 ka BP (e.g., Weninger et al., 2006). But
340   this may have conflated cold indicators from certain regions with arid indicators from
341   other regions (e.g., north of the Aegean Sea, or in high-altitude Anatolia, as seen also for
342   the LIA – see *section 2.2*), and conflated broader (8.6 to ~8.0 ka BP) RCC conditions with

343   those specific of the superimposed 'Hudson Bay event at 8.2 ka BP. Thus, these results
344   need to be approached with care. More recent studies suggest that the abrupt (decadal-
345   scale) onset of Neolithic expansion from Anatolia and the Near East into the Aegean
346   coincided at a decadal scale with the RCC onset at ~8.6 ka BP(e.g., Weninger et al., 2014;
347   Horejs et al., 2015; Krauß et al., 2017). Furthermore, the abrupt (decadal-scale)
348   Neolithic movement out of the Aegean region, both into the Adriatic and SE Europe,
349   coincided with the end of that RCC at 8.0 ka BP. For example, Neolithisation of large
350   parts of the Pannonian Basin was completed within 100 years following the RCC-ending
351   at 8.0 ka BP, and—coming from the Aegean—the Neolithic reached the Iberian
352   Peninsula and Morocco within 200 yrs of the RCC-ending at 8.0 ka BP (e.g., Linstädter et
353   al., 2016). In addition, widespread desertion of archaeological sites occurred in the
354   southern Levant during the 8.6-8.0 ka BP RCC-interval (Gebel, 2009; Rollefson, 2009;
355   Zielhofer et al., 2012; Clare, 2016), and animal husbandry spread from the Levant into
356   NE Africa in coincidence with the RCC-ending at 8.0 ka BP (cf. Kuper and Kröpelin,
357   2006), while painted Halaf pottery started to spread from the northern Levant
358   throughout Mesopotamia at about the same time (e.g., Nieuwenhuyse, 2017; van der
359   Plicht et al., 2011).
360
361   In summary, both the abrupt onset of moist conditions at around 10.2 ka BP, and the
362   return to milder climatic conditions immediately following the 8.6-8.0 ka BP RCC (e.g.,
363   Gkinis et al., 2014), are suggestive drivers of a rapid, punctuated mode of Neolithic
364   dispersal (cf. Van Andel and Runnels, 1995; Guilaine, 2001; Fiedel and Anthony, 2003),
365   rather than the still more widely accepted slow-and-continuous 'Neolithic Wave-of-
366   Advance' dispersal model based on incremental demographic growth (Ammermann and
367   Cavalli-Sforza, 1979). Yet, as mentioned in *section 2.3*, it will be extremely challenging to
368   distinguish archaeological responses to the RCC-style event from those to the wider
369   regional, orbitally forced, climate changes at that time. From 8.0 ka BP onward, climate
370   conditions were less affected by underlying orbital changes.
371
372   An example of post-8.0 ka BP archaeological change that coincided with an RCC
373   concerns the end of the Copper Age in SE Europe. It coincides with the RCC-onset
374   around 6 ka BP, followed by a major 1000-year settlement gap in SE Europe and the
375   Aegean until RCC-end at around 5.2 ka BP (Weninger et al., 2009). Interestingly, during
376   the same RCC, the Ukraine experienced a major settlement expansion, which has been
377   attributed to societal resilience of the (cold-adapted) Cucuteni-Tripolye cultural
378   complex (Weninger and Harper, 2015). Finally, the end of the Bronze Age around the
379   Aegean coincided closely with the regional RCC expression of 3.1-2.9 ka BP (e.g., Rohling
380   et al., 2009; Kaniewski et al., 2010, 2017; Cline, 2014).
381
382   It appears, therefore, that there is a strong temporal relationship between RCCs in the
383   wider eastern Mediterranean region and major archaeological changes, although—even
384   within the Fertile Crescent (e.g., between the N- and S-Levant)—establishing such
385   coincidences is complicated by complex interregional differences in terms of, for
386   example, cultural trajectories, natural biodiversity, landscapes. Local socio-political
387   processes are likely to have always modulated the diverse adaptive strategies of human
388   societies in times of changing climate, suggesting that no generalised associations
389   should be made between societal changes and periods of climate change (Weiberg et al.,
390   2016). Accordingly, this study does not *a-priori* assume that correlation means
391   causation, but seeks to identify why a correlation may be apparent between

392   archaeological records and high-resolution Greenland GISP2 nss [K+] or [Na+] records,
393   or other high-resolution records (e.g. Jeita Cave, speleothem $\delta^{18}O$). In other words, we
394   investigate whether there is a reasonable, replicable physical framework of connecting
395   mechanism(s) that could explain the correlation, which might then be independently
396   tested. This framework should reasonably demonstrate how variations in Greenland
397   records could relate to local palaeoclimate records, and what the inferred process
398   connection would imply for RCC climatic conditions at, and gradients between, different
399   locations in the study region.
400
401   *2.5. This study*
402   Previously inferred climatic impacts on eastern Mediterranean climate for the RCCs
403   remain qualitative and thus difficult to validate robustly. Even straightforward
404   conceptual expectations for the regional impacts of cold NPC air outbreaks over the
405   study region suggest considerable complexity. Following the Clausius-Clapeyron
406   relationship, absolute humidity at saturation is lower in cold air than in warm air. Yet
407   relative humidity can still be high because it relates the actual moisture content to the
408   saturation value at a given temperature. This complicates previously generalised use of
409   "cold and dry" associations (e.g., Valsecchi et al., 2012) because a cold air mass might
410   hold less moisture, but may still drive considerable precipitation and/or fog when
411   temperatures drop and/or air is uplifted. Also, relative humidity is near 100% so
412   evaporation rates will be low at those times. In a practical sense, therefore, no
413   particularly "dry" conditions need to be expected in regions under a cold airflow.
414
415   Things change when such an air mass flows out over a relatively warm ocean or lake
416   surface. Then, its temperature and saturated humidity potential rise, and its relative
417   humidity drops as a consequence. This triggers intense evaporation. In terms of
418   evaporation potential over relatively warm, moist surfaces, therefore, the cold air mass
419   indeed appears "dry". For example, lake levels are likely to drop. But fields and crops
420   bound to growth in the wet season might still receive sufficient net moisture to remain
421   productive (Rohling, 2016), and cold and frost may be more damaging for such systems.
422
423   Following transit of the air mass over water for a few days or more, its moisture content
424   will have been increased strongly due to evaporation. When the air mass subsequently
425   makes landfall and is cooled and/or uplifted, its relative humidity increases and
426   (strong) precipitation may develop. This may fuel suitable conditions for plant and crop
427   growth, or even detrimental (flash) flooding, while lake-levels are likely to rise
428   (depending on the ratio between the lake-water and lake-catchment areas; Rohling,
429   2016). Meanwhile, stable O (and H) isotope ratios of precipitation are affected by initial
430   advection, evaporation, and both temperature fractionation and Raleigh distillation
431   during condensation. Therefore, the overall picture is one of complex and often counter-
432   intuitive relationships that compromise straightforward interpretations of spatial
433   trends and gradients between proxy records.
434
435   This study develops the conceptual formulations above into a first testable, reasonably
436   quantified (signs and approximate magnitudes) template for interpretation of the key
437   environmental expressions of changes between times with more frequent
438   polar/continental air outbreaks over the Aegean-Levantine region (i.e., RCCs), and times
439   with much lower frequencies of such events (i.e., times in between RCCs). For this, we
440   present a physically coherent framework of minimal complexity in the form of a 2-

9

441 dimensional Lagrangian model, which can be easily interrogated. The modelled
442 expectations are first tested against increased cold NPC air outbreak frequencies, which
443 in turn cause Aegean cooling on land and at the sea surface (e.g., Rohling et al., 2002a,b;
444 Kotthoff et al., 2008; Josey et al., 2011; Tolika et al., 2014; Anagnostopoulou et al., 2017).
445 For this exercise, we set the outbreak frequencies as a function of the record of GISP2
446 nssK+ enrichments (O'Brien et al., 1995; Mayewski et al., 2004; Muschitiello et al., 2013),
447 given that this record underlies definition of the (global) RCCs (Mayewski et al., 2004).
448 Next, we explore responses on land, in comparison with terrestrial palaeoclimate
449 reconstructions around the Aegean-Levantine region. Thus, albeit simplified, the model
450 aims to address all processes relevant to the RCC problem, and can therefore reveal to
451 what extent observed proxy signals can be explained by the RCC mechanism of cold NPC
452 air outbreaks over the study region, and to what extent they reflect
453 alternative/additional processes. The model's physically coherent view of regional
454 variability may also benefit research into the impacts of climate change on early
455 societies.
456
457 **3. MODEL**
458 *3.1. Modelling the impact of changing NPC air outbreak frequencies*
459 Here we describe only the general concepts behind our daily-resolved 2-dimensional
460 model (Figure 1); full details are available in the pdf of the graphical MathSoft MathCad
461 13 code, with annotations (Appendix). We do not presume that our model
462 comprehensively captures all processes that act in reality. Instead, it aims at developing
463 a physically coherent view of changes in the key environmental parameters over
464 representative distances, in idealised scenarios related to variations in the winter-time
465 RCC mechanism of cold NPC air outbreaks over the Aegean-Levantine region.
466
467 Our model does not account for long-term, orbital-scale hydrological changes in the
468 study region (e.g., Tzedakis, 2007; Rohling et al., 2015; Bosmans et al., 2015). It only
469 considers anomalies relative to modern conditions through the year, related to NPC
470 outbreaks of varying frequency during winter. Specifically, it resolves the influence of
471 10-day cooling and increased-wind-speed- anomalies that are superimposed upon the
472 winter half-year of a regular (sinusoidal) annual cycle. Results are considered relative to
473 a "control" year, which is set to be a year with 1 of these anomalies. A year with no
474 anomalies then is milder than the control year, and years with 3 or 5 anomalies are
475 more severe than the control year. The same cooling anomalies are applied where the
476 airflow makes landfall (see below).
477
478 Initial air properties (which enter the Aegean region from the north) are set using an
479 idealised sinusoidal representation of the annual cycle with air temperature (T_a),
480 relative humidity (r), and vapour $\delta^{18}O$ (δ_a; calculated based on vapour-liquid
481 fractionation from northern Greece rainfall $\delta^{18}O$), following representative ranges of
482 observations of 1 to 23 °C, 0.45 to 0.75, and –22 to –16 ‰, respectively
483 (Climatemps.plovdiv; Climatemps.alexandroupoli; Dotsika et al., 2010). Wind speed (V)
484 is set with a sinusoidal function that shows a double peak each year (one in summer and
485 one in winter) over the Aegean region, between 5 and 7 ms^{-1} (Weatherspark). Surface
486 absorbed insolation is set with a sinusoidal curve over a range of about 60 to 300 Wm^{-2},
487 based on modern values for Athens (about 50-230 Wm^{-2}; Carletti et al., 2014) but
488 allowing cleaner pre-anthropogenic and non-city atmospheric conditions, especially in
489 summer. Air properties are considered within an exchange layer of thickness D, which

490 sinusoidally cycles between 1 km (summer) and 1.4 km (winter) (within ranges
491 reported by Dayan and Rodnizki, 1999; Seidel et al., 2012; Dayan et al., 2017), and all
492 mean properties (e.g., air temperature, vapour pressure, density, pressure) are
493 calculated with respect to the value of D that applies at the specific moment in the
494 seasonal cycle. Change in the settings for D would need to be compensated by changes
495 in the model's tuning parameters, which are set once for the present and then kept
496 constant, so changes in D do not materially affect our results. Vertical air displacements
497 in the model affect air temperature by means of a simple moist adiabatic lapse rate set
498 to –6.5 °C/km (within the ranges given by Alpert et al., 1989; Vardavas et al., 1997;
499 Dayan et al., 2002; note that minor changes in this value are again neutralised during
500 tuning of the model's air uplift values to give correct "control" P values—see below).
501
502 During passage over the sea, evaporation adds water from the sea into air layer D, with
503 fluxes calculated in daily increments after Rohling (1999) and Rohling et al. (2004). The
504 airstream then makes landfall at Crete, and passes over it, at which time it is uplifted by
505 5000 m during the (10-day) events of cold air outbursts over the relatively warm seas,
506 given that this is known to cause strong atmospheric instability that leads to
507 thunderstorms with intense precipitation and stable isotope fractionation (the uplift
508 height is set after modern observations; Altaratz et al., 2001; Galvin et al., 2011; Ben
509 Ami et al., 2015). Next, the partially rained-out airflow undergoes dry adiabatic descent
510 back to sea level at ~10°C/km, and thereafter flows across the Levantine Sea at mean (')
511 velocity $V_{H'} = (V + V/s_H)/2$. Here, s_H (in the code, $spacH$ where H stands for Haifa) is a
512 tuning factor that spreads the airflow over a larger spatial domain in the Levant so that
513 simulated rainfall amounts for a control year approximate observed values, for eastern
514 Levantine air uplift heights that are constrained by modern observations (~6500 m for
515 the Cyprus Low; Ganot et al., 2007). In both regions, modern annual precipitation values
516 are about 500 mm (Climatemps.crete; Climatemps.haifa). Deep convection
517 (thunderstorms) associated with the Cyprus Low is the main mechanism for strong
518 precipitation in the region (Tarolli et al., 2012). This strong uplift again causes intense
519 precipitation and stable isotope fractionation. Use of the tuning value s_H in $V_{H'}$ ensures
520 conservation of mass in the airflow; s_H is set once for a control year and then kept
521 constant throughout.
522
523 The model also allows a measure of air uplift at times outside the cold events, which is
524 set empirically using a sinusoidal function, between a winter maximum of 1220 m and a
525 summer minimum of 0 m. The winter maximum value represents a fine-tuning factor
526 that empirically sets rainfall over Crete in a control year to observed values
527 (Climatemps.crete). The summer-time zero value represents a crude approximation of
528 summer-convection inhibition by mid-tropospheric descent (Tyrlis et al., 2013 and
529 references therein). These, and a number of other parameterisations in the model setup,
530 are rather subjectively selected within reasonable ranges, but they are warranted
531 because our objectives are not about modelling reality. Instead, we tune settings to
532 modern observed values for control years, and then only consider what relative changes
533 would take place during anomalous years with an otherwise identical model setup.
534
535 After entering the study region, the air in the model flows out over a mixed layer of
536 seawater of constant thickness (set to 100 m), with an initial sea-surface temperature
537 (SST) that varies through the year with a sinusoidal function between fixed seasonal
538 extremes of 13 and 23 °C (Rohling et al., 2002b and references therein), and with initial

539   seawater salinity (*SSS*) of 39 and $\delta^{18}O$ (δ_s) of 1.5 ‰. Air-sea interactions change all
540   three properties through time in the model. After a model year, these properties are
541   reset to their initial values, in an approximation of the influence of large-scale spatial
542   mixing/advection. If a degree of "memory" of the preceding year's changes were
543   included, then the amplitude of simulated changes would be enhanced, so our simulated
544   amplitudes should be considered as minimum estimates. The passage-time of air over
545   the sea is calculated using wind speeds in combination with a scale factor for the N-S
546   distance over the Aegean Sea and the ESE distance from Crete to Israel over the eastern
547   Levantine Sea. We use ~1400 km for the total distance from the north Aegean to the
548   Israeli coast near Haifa, and simply consider that Crete splits this into two equal halves.
549   For both landfall locations (Crete and Israel/Haifa), air temperatures at sea level are set
550   using sinusoidal annual cycles between observed seasonal extremes (Climatemps.crete;
551   Climatemps.haifa; Climatedata). The amplitudes of temperature anomalies during
552   superimposed 10-day events at both Crete and Israel/Haifa are set equal to those in the
553   initial airmass that enters the study region.
554
555   The model simultaneously resolves changes in *SST*, sea-surface salinity (*SSS*),
556   evaporation and the stable oxygen isotope ratio of evaporation (E, δ_e), the time-
557   dependent development of the moisture content of air and its stable oxygen isotope
558   composition (δ_a; including Rayleigh distillation when precipitation occurs),
559   precipitation and its stable isotope ratio (P, δ_p, also considering Rayleigh distillation),
560   net freshwater fluxes at sea level ($E+P$), snowline (0 °C) altitude, negative degree-days
561   at a set altitude (chosen at 2000 m to gauge longer-term snow preservation potential on
562   the high mountains), and lake-level changes for hydrological changes at sea level at two
563   hypothetical lake sites (one in Crete and one in Israel) as well as a Dead-Sea-like basin
564   (see *section 3.2*).
565
566   E and δ_e are calculated as outlined in Rohling (1999) and Rohling et al. (2004), except
567   that the ratio of resistance coefficients is not set at 1.0142 in the δ_e calculation
568   (Gonfiantini, 1986), but at a lower value of 1.010 (others have similarly used a lower
569   value: Merlivat and Jouzel, 1979; Gat, 1996); thus, annual mean δ_p in both Crete and
570   Israel in a control year is close to –6 ‰, in approximate agreement with observations
571   (Rozanski et al., 1993; Argiriou and Lykoutis, 2005; Dirican et al., 2005; Gat et al., 2005;
572   Dotsika et al., 2010). P is determined based on the local surface temperature and uplift-
573   related air temperature, pressure, and density changes and their impacts on saturation
574   vapour pressure; for any given airflow with a certain moisture load, these changes
575   cause relative humidity to increase as uplift occurs, until relative humidity reaches 1, at
576   which time precipitation occurs so that relative humidity is kept at 1 (it does not exceed
577   saturation). The value of δ_p is calculated from the air-vapour ratio (δ_a) using
578   condensation-temperature-dependent equilibrium fractionation (Majoube, 1971),
579   combined with co-evolution of δ_p and δ_a due to Rayleigh distillation when precipitation
580   occurs. After dry adiabatic descent back to sea level following the uplift over Crete, the
581   air flow with its remaining moisture (and end-member δ_a) flows over the eastern
582   Levantine Sea, where it again gains moisture due to E (and δ_e), until uplift and cooling
583   over the Levant, where P and δ_p are calculated in the same manner as outlined before
584   for Crete. For full details and further references, see the code provided.
585
586   Model performance for various ranges of event temperature and wind speed is
587   evaluated in Figure 2. This provides basic set-up values for these parameters, which are

588 evaluated for realism relative to observations, and which are then kept constant
589 through all runs. That is, only the frequency of events is changed thereafter.
590
591 The above provides a single, physically coherent framework for calculating – for years
592 with 0, 1, 3, or 5 cold outbreak events per winter – the *SST* and *SSS* changes in the ocean
593 mixed layer, as well as winter, summer, and annual mean values for *E* and *P* in Crete and
594 Israel, with attendant δ_p values (and the size of the amount effect). In addition, the
595 calculations give snowline altitudes in Crete and in the Levant, and negative degree-
596 days at 2 km altitude in the mountains. These all become input parameters in our next
597 exercise: to create a Holocene time-series of climate impacts using the GISP2 nssK[+]
598 time-series as a template for frequency changes of cold NPC air outbreaks (Rohling et
599 al., 2002b).
600
601 ### *3.2. Generating time-series of Holocene variability*
602 To generate the Holocene time-series, the model divides the raw 3-year-resolution
603 GISP2 nssK[+] time-series (Mayewski et al., 1997; Rohling et al., 2003) into classes, where
604 <50, 50-80, 80-95, and >95 percentile values were related to years with 0, 1, 3, or 5
605 events per winter, respectively (Figure 3a). This year-type record was then used to
606 make a time-series of characteristics as modelled for each year-type. We then smoothed
607 these resultant 3-year-resolution time-series of modelled parameters as appropriate for
608 the temporal resolution of each type of proxy record in palaeoclimate studies that is
609 equivalent to one of our modelled parameters. Mostly, we use 50-y Gaussian smoothing
610 to highlight major patterns of change. However, simulated records of Aegean SST (and
611 SSS) change were smoothed with a 200-y Gaussian window, to match marine proxy
612 records (Figure 3c,d). The model primarily determines lake-level variations at the
613 original output resolution because these are cumulative signals over time, and then
614 smooths the resultant cumulative records with a 50-y Gaussian window (Figure 3g).
615
616 We also calculate first-order approximations for changes in cave-water and cave-
617 carbonate oxygen isotope ratios, using δ_p and δ_c, where the latter accounts for the
618 water-carbonate fractionation effect of mean temperature changes (Figure 3h,i). These
619 records are presented for the Levant based on the property simulations for Israel/Haifa,
620 and were smoothed with a 20-y Gaussian window to visually compare the calculated
621 variability with that observed in records from Jeita Cave in Lebanon (Cheng et al., 2015)
622 (Figure 4a).
623
624 The idealised lakes resolved within the model each have a variable lake area within a
625 constant catchment area, which are proportionally related as 1:($\Phi_{(t)}$−1), where
626 $\Phi_{(t)} = (A_{catchment} + A_{lake(0)})/A_{lake(t)}$. Here, the base value of Φ (i.e., $\Phi_{(0)}$) is set in such a way
627 that the lake is at steady state (zero change) for the climate parameters of the present-
628 day "control" year (a 1-event year). We simply assume that all *P* onto the catchment
629 area immediately enters the lake without evaporative loss; thus, evaporative loss occurs
630 only from the lake surface area itself. In essence, the modelled lakes occupy perfectly
631 conical depressions, where the catchment area is represented by the maximum opening
632 of the cone minus the time-dependent area of the lake within the conical depression. We
633 specify for each lake a standard depth of 30 m for the present day, and set the slope of
634 the conical depressions to 1 degree. Changes in the lake-slope angle strongly affect the
635 initial lake area—and via $\Phi_{(0)}$ also the catchment area—but simulated lake-level

636 variations are not significantly affected. The calculated past lake-level-changes are
637 shown relative to the model's simulated present-day lake-level value.
638
639 Finally, we calculate lake-level variations for a Dead Sea-like basin, using a simplified
640 version of the basin's area-to-depth ratio after Rohling (2013) (for details, see the code
641 provided) and $\Phi_{DS(0)}$ = 40 after the same study (Figures 3g,4c). Further simplified
642 representations after Rohling (2013) that are applied in the current model's Dead Sea-
643 like case are: (*a*) a high-salinity-driven ~50% reduction in the rate of evaporation from
644 the basin, relative to evaporation from pure fresh water; and (*b*) a value of ~3 for the
645 ratio P:$P_{preserved}$, where $P_{preserved}$ stands for the amount of P from the wider catchment
646 area that makes it into the lake following loss through evapotranspiration (for details,
647 see code provided). The model simulates a record of climate-imposed changes in the
648 level of water within a Dead Sea-like basin, which then is normalised to 0 m for the
649 present-day level.
650
651 There are some important caveats. First, as mentioned before, the model does not
652 account for underlying astronomically forced variations in the region, given that the
653 GISP2 nssK$^+$ Holocene record (used as input for our model) is dominated by variations
654 at centennial to millennial timescales (O'Brien et al., 1995; Mayewski et al., 2004;
655 Muschitiello et al., 2013). Second, all simulated records show variability related to only
656 the wintertime RCC component considered, and ignore other influences resulting from,
657 for example, summer droughts, and/or westerly or (south-)easterly air flows.
658 Consequently, perfect representation of observed palaeoclimate proxy records and of
659 their full centennial- to millennial-scale climate variability cannot be expected. Finally,
660 we emphasise that the model output is especially focussed on comparison with records
661 close to the simulated regions of precipitation, evaporation, and frost and snow
662 potential (notably Crete and Levantine coastal to mountainous regions).
663
664 **4. RESULTS**
665 The modelled apparent interannual isotopic "amount effect" is determined similarly to
666 how it affects stable oxygen isotopes recorded in a cave, namely in terms of the ratio
667 between annual mean change in δ_p over annual mean change in P, between different
668 years. We determine the amount effect as the mean of the two values of $\Delta\delta_p/\Delta P$ for a
669 three-event year relative to a "control" year, and a five-event year relative to a "control
670 year". Values are expressed as stable oxygen isotope difference per 100 mm of rainfall.
671
672 Our results identify the magnitude of cooling during each 10-day cold event as the most
673 important control on the apparent interannual isotopic "amount effect" for Israel
674 (Figure 2a, filled dots). This is not so much because of fractionation and Rayleigh
675 distillation, but mainly because the magnitude of cooling has strong influences on both
676 the amount of moisture held in the incoming air (lower for colder events), and the
677 amount of evaporation from the sea (greater for colder events). The importance of this
678 complex and somewhat counter-intuitive mixing—in shifting proportionalities—
679 between advected (external) and evaporated (Mediterranean) moisture casts doubt
680 over qualitative assumptions about how changes in rainfall isotope compositions
681 extrapolate across the wider region. Significant non-linearities in these relationships
682 should be expected, so that quantitative evaluations are essential for good
683 reconstructions.
684

14

685   We identify the most representative initial cooling intensity for all events by
686   comparison of the model's apparent interannual isotopic amount effect with that
687   observed in Israel (Figure 2a, filled dots). Observations for Soreq Cave, Israel, imply a
688   value of about –0.5 ‰ per 100 mm of rainfall (Bar-Matthews et al., 2003). This is best
689   approximated (within uncertainties) by the model for mean air-cooling during cold
690   events of ~9 °C (Figure 2a, heavy dashed arrow). For that value, there is also a good
691   agreement with the individual P amounts (open diamonds) and δ_p values (crosses) for
692   both Crete and Haifa (Figure 2a). Accordingly, we set our main experiment to run with
693   cooling amplitudes of 9 °C for each of the 10-day cold events. For the Cretan site, we
694   simulate only a minor amount effect (0.14 ‰ per 100 mm of rainfall), which agrees
695   with an apparent lack of correlation between δ_p and P reported for that location by
696   Argiriou and Lykoutis (2005). That observation in Crete by itself indicates already that
697   the classic interpretation of the apparent "amount effect" in the Levant may be
698   questionable, because a similar, or at least systematically other, amount effect would
699   then be expected in relatively nearby locations like Crete. The fact that our model finds
700   coherence of simulated and observed differences between Crete and the Levant
701   suggests that it offers a more realistic explanation of the apparent amount effect. Hence,
702   as stated above, straightforward interpretations of regional δ_p changes in terms of P
703   changes through fractionation and Rayleigh distillation should be considered with
704   significant caution; instead, changes in the balance between advective and evaporative
705   moisture fluxes may be dominant.
706
707   Because evaporation rates are linearly related to mean wind speed, we assess the
708   impacts of wind-speed changes as well (Figure 2b). We find that the impacts of wind-
709   speed changes on most parameters cancel out over the sea because travel time along
710   the trajectories is inversely proportional to mean wind speed. Yet mean wind speed still
711   affects annual cooling of the marine mixed layer. Long-term RCC expressions in the
712   basin suggest cooling of ~2 °C, up to 3 °C (see above). Such values are suggested by the
713   model's 200-year-smoothed annual SST anomalies when the wind-speed anomaly
714   during cold events (V) is set to about +10 m s^{-1} (Figure 2b). This value agrees with the
715   aforementioned observations of northerly outbreak velocities from 17 to 25 m s^{-1},
716   which imply anomalies of at least 10 m s^{-1}.
717
718   Modern observations, highlighted before, corroborate our inferred mean cooling
719   amplitudes of the order of 9 °C (see code provided for various diagnostics from our
720   main scenario). During cold NPC air outbreaks, cooling by ≥4 °C occurred in Bulgaria
721   and in the Alps, and observations in central Greece go as low as –20°C. In addition,
722   observations of enhanced preservation of snow on Cretan mountains (which reach up
723   to 2500 m) agree with strong negative-degree-days amplitudes calculated for high
724   Cretan altitudes (Figure 3b). With mean cooling amplitudes of the order of 9 °C, the
725   model also suggests snow-line drops to altitudes of 770 and 920 m for the Levant and
726   Crete, respectively, which are coherent with snow events observed in Jerusalem (787 m;
727   see also below). In addition, modern observations during cold events report deep frosts
728   (and snow) at low altitudes in the northern Aegean (e.g., Thessaloniki) and Bosporus
729   regions, in agreement with the model's event-mean minimum temperatures down to –
730   8°C in regions north of the Aegean. This is consistent also with air temperatures in
731   2001, which were still as low as 0 to –2°C after passing a considerable distance over the
732   relatively warm northern Aegean Sea (Casford et al., 2003). Within each event, there

733   may be colder spikes, but these are not resolved; our model's 9°C cooling anomaly
734   represents the mean for an entire 10-day event.
735
736   The modelled amplitudes of precipitation change also help in validating the model's
737   performance. For both Crete and Israel (Haifa), the model returns values of 505 mm y^{-1}
738   for the present control year (unsurprisingly, given that the model's settings are tuned to
739   these control-year values). In a year with 5 cold events, the model infers an annual P
740   amount of 798 mm for Crete and 777 mm for Israel. Five cold events in the model
741   amount to 50 days, which is 40 more than in a control year with one 10-day event. For
742   both locations, that implies roughly 7 mm of extra rain per day, assuming that it rains all
743   day, every day, and that all rain is spatially equally distributed. In reality, there is
744   inhomogeneity, with locally and temporally intensified bursts of rain that alternate with
745   dry/drier spells. Even over relatively small distances, spatial focusing (e.g., orographic
746   effects) imparts factor-3 differences between high and low rainfall values (Shamir et al.,
747   2016). Over larger distances, such contrasts are likely to be stronger. And temporal
748   focussing also occurs, where some regions stay dry while others receive most of the
749   rainfall. If we tentatively allow for a reasonable range of 3× to 10× combined spatial and
750   temporal focussing of P during the events, then local peak daily rainfall values of ∼20 to
751   ∼70 mm might be anticipated from the model results, which we compare below with
752   modern reported extreme rainfall events.
753
754   On 13 December 2016, heavy downpours hit Israel, with rainfalls up to 10 mm
755   (Timesofisrael). On 25 November 2014, more than 40 mm of rain fell on many regions
756   from North to South through Israel (Israelnationalnews), while a persistent storm in the
757   earliest days of November 2015 brought rainfalls between 80 and 150 mm over 7 days
758   (daily averages of ∼11 to ∼21 mm) (Israelnationalnews). Unusually heavy rainfall of up
759   to 50 mm fell within a day at many places in Israel on 10-11 December 2013,
760   accompanied by northerly winds and unseasonably cold conditions (Floodlist). Such
761   storms are often associated with snow, especially on the higher mountains (e.g., Mount
762   Hermon in the north, ∼2800 m high), but also extending much lower (e.g., up to 15 cm
763   in Jerusalem at 787 m altitude, in January 2013; Dailymail). In view of these reports, our
764   simple model does a reasonable job at approximating the scale of P increases associated
765   with the cold events. The weather reports also validate our simulated event-average
766   drops in snowline-altitudes, down to the altitude of Jerusalem.
767
768   With respect to lakes, the model investigates identical idealised lake shapes at sea level
769   in both Crete and Israel. In both cases, the assumed initial lake depth of 30 m and
770   lakeside slope of 1 degree geometrically determine the initial lake diameter (3437 m)
771   and lake surface area (9.28×10^6 m^2). The size of each lake's catchment area is found via
772   region-specific multiplier $\Phi_{(0)}$. For the calculated control-year conditions, $\Phi_{(0)}$ = 2.27 for
773   Crete, and $\Phi_{(0)}$ = 1.92 for Israel, giving total (catchment+lake) areas of 2.11×10^7 m^2 and
774   1.78×10^7 m^2, respectively (see code for details). Once determined for the present
775   control year, these total areas are kept constant throughout the model runs because the
776   total catchment area in nature relates to a topography that is invariant on the short
777   timescales considered here. The proportion of the total area that is made up by the lake
778   itself fluctuates with lake-level changes, which relate to each year's simulated
779   hydrological conditions. By specifying exactly the same lake shape for both regions, and
780   setting both up so that they are at steady state in a control year, we can directly

781   compare and contrast the lake-level responses to regionally different consequences of a
782   single set of imposed climatic perturbations.
783
784   The lake-level simulations (Figure 3g) show that, as a rule of thumb, periods with
785   no/fewer cold events result in lake-level drops, and periods with more cold events
786   result in lake-level rises. Lake-level minima and maxima, respectively, follow such
787   episodes with lags of a few decades for lakes of the dimensions used here. This is
788   because lake levels represent an integrated signal of preceding non-steady-state
789   conditions in the catchment's E-P balance (i.e., the underpinning connection is between
790   prevailing climate conditions and the *rate* of lake-level change). Within uncertainties,
791   the specified systems respond very similarly in Israel and Crete (Figure 3g red, blue).
792   But we emphasise that real-world examples require careful definition of the time-
793   variable lake-surface-area occupation of part of the total surface area ($\Phi_{(t)}$). This
794   requires use of detailed digital elevation models and lake-level and drainage
795   assessment, since $\Phi_{(t)}$ is a critical term for case-specific lake-level responses (see also
796   Rohling, 2016).
797
798   The simulated level variations in the model's Dead Sea-like basin (Figure 3g, green) are
799   similar to those of those in the two idealised lakes, but with larger amplitudes that are
800   specifically characterised by proportionally stronger lake-level drops. These differences
801   arise predominantly from the much larger ratio of catchment area to lake area (Φ) in
802   the Dead Sea-like case, and from the high $P{:}P_{preserved}$ ratio applied to the basin which
803   considerably increases the $E{:}P$ balance.
804
805   Simulated fluctuations in δ_p are of similar sign for Crete and Israel, but their amplitudes
806   are very different (Figure 3f). Conversely, the simulated amplitudes of P changes are
807   similar between Crete and Israel. This implies that the amount-effect ratio of $\delta_p{:}P$ varies
808   considerably between sites (see above).
809
810   **5. DISCUSSION**
811   The simulated Holocene climate variability, using GISP2 nssK$^+$-based variations in event
812   frequencies, reveals a pattern that consists of a relative flat "background" with distinct
813   multi-decadal to centennial-scale anomalies (Figure 3). This pattern, without long-term
814   orbital modulation, arises from the approach followed (*section 3*), which is not designed
815   to capture orbital-scale changes, but focuses on RCC anomalies only. Accordingly, the
816   output of our model can only be used to compare climate anomalies during the RCCs
817   with times in between the RCCs. The simulated time-series capture to a remarkable
818   degree the multi-centennial variability seen in time-series of proxy climate data for the
819   region, and specifically that in SST records (e.g., Abu-Zied et al., 2008; Clarke et al.,
820   2016; Gogou et al., 2016; Kuhnt et al., 2007; Marino et al., 2009; Rohling et al., 2002a,b)
821   (Figures 3c, 5). This implies that the fundamental nature of the observed temperature
822   records is well represented by the model, and that the RCC mechanism of northerly air
823   outbreaks is a key driver of interannual to multi-centennial Aegean SST variability (as it
824   still is today; e.g., Josey et al., 2011).
825
826   The model simulates both increased P and decreased δ_p in Crete and Israel during
827   periods with a higher frequency of cold northerly outbursts (Figure 3e,f). Decreases in
828   δ_p are conventionally interpreted as periods with increased P. Because the sign of δ_p
829   variations is the same for Crete and Israel, palaeoclimatic interpretations based on δ_p

17

830   variations would therefore offer the same (qualitatively consistent; see Figure 3f)
831   conclusion that RCC-like episodes with higher frequencies of cold events in the region
832   coincided with increased P. This would apply at all locations where the cold (and thus
833   initially relatively dry) airstream makes landfall after gaining moisture during a
834   substantial transit over the evaporative Aegean and Levantine Seas. In quantitative
835   terms, however, the amount of P that corresponds to a given unit of change in δ_p differs
836   strongly from site to site on regional scales (see contrast between Crete (blue) and
837   Israel (red) in Figure 3f). Hence, it appears that δ_p is not a good tool for straightforward
838   mapping of patterns of P; physically coherent, quantitative assessment (modelling) is
839   essential to such exercises.
840
841   There is some qualitative support from palaeoclimatic reconstructions for the model's
842   expected regional P increases during RCC events. Certain RCCs (especially that at
843   around 8 ka, but also the LIA) bear evidence of intervals of sharply increased
844   precipitation/runoff, including rubble/mud slides and flash-flood deposits (e.g., Xoplaki
845   et al., 2001; Bar-Matthews et al., 2003; Peyron et al., 2011; Lespez et al., 2013; Berger et
846   al., 2014). Boyer et al. (2006) reported a flooding phase on the Konya plain, Anatolia,
847   with a calibrated radiocarbon date in the range of 8.75-8.45 ka BP (extending to ~9-8 ka
848   BP based on datings in another section). This was later interpreted by Roberts et al.
849   (2016) in terms of enhanced spring snowmelt following cold winters with increased
850   snow cover, along with less precipitation in other seasons.
851
852   In contrast, stable hydrogen isotope data (which behave comparably, albeit not
853   identically, to stable oxygen isotopes in the hydrological cycle; Hoefs, 1997), measured
854   on vegetation remains from northern Greece, suggest aridification at 8.7-8.2 ka BP,
855   followed by a sharp reversal to surface wetness at 8.2-8.0 ka BP (the "8.2 ka" Hudson
856   Bay flooding event) with a subsequent gradual increase in surface wetness until 7.5 ka
857   BP (end of the reported study) (Schemmel et al., 2016). Note, however, that the rainfall
858   regime over northern Greece is not predictable using the system evaluated here, given
859   that this regime does not strongly depend on winter-time passage of northerly airflows
860   over the Aegean-Levantine Seas and subsequent uplift upon landfall, so we refrain from
861   further discussing records from this sector of the Aegean region (Kotthoff et al., 2008;
862   Pross et al., 2009; Schmiedl et al., 2010; Schemmel et al., 2016).
863
864   Besides SST, the most convincing and consistent corroboration for the model results
865   comes from the very highly resolved and precisely dated cave-speleothem $\delta^{18}O$ record
866   from Jeita Cave, Lebanon (Cheng et al., 2015) (Figures 4a, 5). The relatively nearby
867   record for Soreq Cave, Israel, is of generally lower and irregular resolution through the
868   Holocene (Bar-Matthews et al., 2003; Bar-Matthews and Ayalon, 2011), so we focus on
869   Jeita Cave. The Jeita Cave speleothem $\delta^{18}O$ record was originally interpreted in terms of
870   correlation to so-called Bond events in the North Atlantic, but a physical process link
871   remained to be quantitatively demonstrated. Given that Bond events show a rough
872   correlation with RCCs as determined from the GISP2 nssK[+] record (Mayewski et al.,
873   2004), we here compare the output of our RCC model with the centennial-scale
874   component of the Jeita Cave $\delta^{18}O$ record. Specifically, we compare our temperature-
875   corrected speleothem carbonate $\delta^{18}O$ approximation (δ_c) with a high-pass filtered
876   record of Jeita Cave (Figure 4a), which highlights the short-term (sub-millennial)
877   fluctuations and removes the underlying, long-term trend related to the general
878   Holocene climate evolution of the Levant that is not accounted for in our model. The

879 Jeita Cave $\delta^{18}O$ residual record is highly dynamic on centennial and shorter timescales
880 (Figures 4a,5). On the whole, on centennial scales, we observe a striking agreement
881 between RCCs, our expected δ_p and δ_c trends for Israel (Figure 3f, red), and negative
882 Jeita Cave anomalies $\delta^{18}O$ (Figures 4a,5). Even the high-frequency variability in our
883 simulated δ_c record shows remarkable similarity with the high-pass Jeita Cave $\delta^{18}O$
884 residual record (Figure 4a).
885
886 These agreements indicate that our simple model's representation of a key climate
887 mechanism in the study region not only simulates well-documented multi-centennial
888 SST variability, but also provides a sound first-order quantitative understanding of
889 centennial-scale (and shorter) P, δ_p, and cave-δ_c variations in the Levant (Figures 3–5).
890 Note that our simulated δ_c record for Israel (Figure 3h) by design only captures
891 anomalies related to the winter-time RCC mechanism that is considered. Given that this
892 fails to explain the positive Jeita Cave anomalies (Figure 4a, grey), we infer that the
893 Middle East was affected by a second dominant climate mode in the region; possibly,
894 droughts associated with (summer-time?) extension of evaporative subtropical
895 conditions, which may also underpin, for example, the droughts documented in Iran
896 during some RCCs (Sharifi et al., 2015).
897
898 Our calculations for lake-level variations in a Dead Sea-like basin present a systematic
899 pattern of highstands during RCCs (Figure 4c). This conflicts with reconstructions for
900 the actual Dead Sea, which show a more complex suite of responses (e.g., Migowski et
901 al., 2006; Torfstein et al., 2013a,b) (Figures 4c). Unfortunately, however, some of these
902 reconstructions show a major peak at around 6.0 ka BP (Torfstein et al., 2013a,b; Kagan
903 et al., 2015), while this is conspicuously absent from other reconstructions (Migowski et
904 al., 2006; Litt et al., 2012). We have failed to find an in-depth debate and consensus on
905 this issue (cf., Zielhofer and Weninger, 2013; Stein and Litt, 2013). Once a consensus
906 Dead Sea reconstruction emerges, we propose that the difference between this record
907 and our hypothetical simulation might be used to evaluate climatic impacts on the real
908 basin that are overlooked in our model, similar to our assessment of the positive Jeita
909 Cave anomalies.
910
911 Finally, we summarise recent syntheses of climate events around the study region in
912 Figure 5. Within the RCC bands, and especially the tighter intervals of the regional
913 eastern Mediterranean RCC expressions (Rohling et al., 2002b), arid signatures seem to
914 be rarely reported. When they are, such arid signals are mostly seen in: *(a)* the North
915 Aegean sector, at the upstream side of our northerly airflow mechanism, for the RCC of
916 8.6-8.0 ka BP (though it changes to a wetter expression from 8.2 ka BP; Schemmel et al.,
917 2017); *(b)* several intervals around the region within the RCC of 6-5 ka BP (in the
918 Holocene climate compilation of Clarke et al. (2016) that includes the data from Roberts
919 et al. (2011)); and *(c)* several RCCs in high-altitude Anatolia (Figure 5). Most other
920 reported relatively arid intervals fall outside the RCCs.
921
922 It is difficult to perceive a systematic pattern from such a scattering of information
923 (Figure 5), especially because different proxies have been interpreted in different ways,
924 and because age models are not always very precise. In contrast, the agreement
925 between our model output and the Jeita Cave record of Cheng et al. (2015) convincingly
926 argues that more humid conditions reached from the northwest into the Levant during
927 the RCC intervals, as discussed above. In short, our synthesis implies that most arid

928 events reported from locations downstream of the cold NPC mechanism fall *in between*
929 the RCCs, and that RCCs in such locations were the more humid intervals.
930
931 The aforementioned indications (Figure 5) that climatic signatures on the Anatolian
932 highlands may have been roughly opposite to those in the (lower altitude) rest of the
933 study region may be of regional climatological significance. We propose that high-
934 altitude Anatolian conditions were more directly related to the initial continental
935 conditions found to the north of the Aegean Sea, than to those in the low-altitude
936 atmospheric mixed layer over the Aegean/Levantine Sea where marine evaporation
937 plays a key role. This would be supported by extensions of intensely cold Eurasian
938 continental air masses over the Anatolian highlands during severe winter cold snaps of
939 recent years (e.g., Coulter, 2012).
940
941 **6. CONCLUSIONS**
942 We present a simple 2-dimensional Lagrangian model to evaluate the nature of climate
943 variability in the Aegean/Levantine region during the Holocene RCCs, with implications
944 for major archaeological turn-over events in the region. Our model simulates the
945 impacts of frequency changes in winter-time northerly air outbreaks over the study
946 region (the "RCC mechanism") on key climate parameters, such as: sea-surface
947 temperature and salinity, evaporation and stable oxygen isotope ratio of evaporation;
948 time-dependent development of the moisture content of air and its stable oxygen
949 isotope composition; precipitation and its stable isotope ratio, net freshwater fluxes at
950 sea level; snowline altitude; negative degree-days at 2,000 m to gauge longer-term snow
951 preservation potential on the high mountains; and lake-level changes for hydrological
952 changes at sea level in both hypothetical lakes and a Dead-Sea-like basin.
953
954 Our model corroborates the notion that RCCs were regionally cold intervals (notably,
955 cold winters) and indicates that the predominant climatic impacts of this winter-time
956 mechanism were "cold and wet," in contrast with intercalated non-RCC "warm and arid"
957 conditions, in the regions downstream of the Aegean and Levantine Seas. To be more
958 specific and precise, the RCCs were periods of highly variable conditions, with an overall
959 tendency toward cold and wet conditions with potential for flash flooding and for
960 episodic snow-cover at low altitudes, at least in the lower-altitude (lower 1 to 1.5 km)
961 regions of Crete and the Levant. The warm and arid intervals in between RCCs require
962 further investigation; we tentatively propose that another mode of climate variability in
963 the region may involve (summer-time?) extension of evaporative subtropical
964 conditions.
965
966 Our results also imply that the "amount effect" observed in Levantine cave $\delta^{18}O$ (and
967 precipitation or drip-water $\delta^{18}O$) does not reflect the conventional concept related to
968 temperature-dependent fractionation and Rayleigh distillation. Instead, it arises
969 because the magnitude of cooling changes the mass-balanced mixing between the
970 amount of moisture held in the incoming air (lower for colder events), and the amount
971 of moisture added due to evaporation from the sea (greater for colder events). The
972 importance of this complex and somewhat counter-intuitive mixing—in shifting
973 proportionalities—between advected (external) and evaporated (Mediterranean)
974 moisture casts doubt over qualitative assumptions concerning the spatial application of
975 a certain "amount effect" through the study region. This is well-illustrated by modern

976 observations of a negligible "amount effect" in Crete *versus* a distinct "amount effect" in
977 Israel. In short, fully quantified evaluations are essential for good reconstructions.
978
979 Finally, our results illustrate that apparent covariations between warm/cold and
980 arid/wet conditions for any given climate event should not be expected to apply over a
981 wide region, but instead are likely to differ spatially, and possibly also with altitude.
982

987
988
989
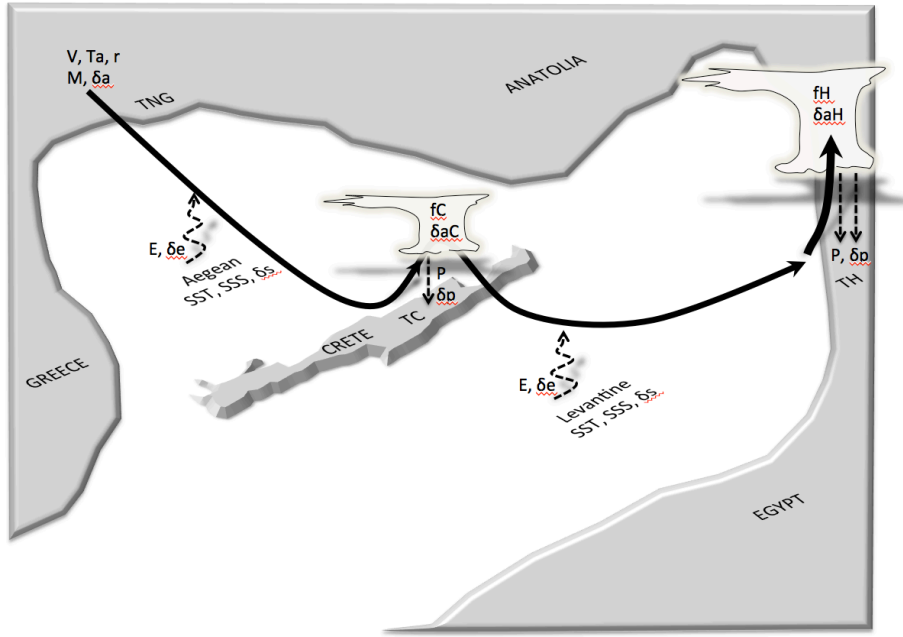
Figure 1. Sketch of the model. V is wind speed. T_a is air temperature, r is relative humidity, M is moisture/vapour mass, δ_a is the O-isotope composition of the vapour, E is evaporation (in m per unit area), δ_e is the O-isotope composition of the vapour added by evaporation, f_C is the fraction of remaining vapour after rainout over Crete, δ_{aC} is the O-isotope composition of the remaining vapour after rainout over Crete, P is precipitation (in m per unit area), δ_P is the O-isotope composition of precipitation, f_H is the fraction of remaining vapour after rainout over Haifa (Israel), δ_{aH} is the O-isotope composition of the remaining vapour after rainout over Haifa. SST is sea surface temperature, SSS is sea surface salinity, δ_s is the sea surface O-isotope composition, all in mean values for a mixed layer of 100 m thickness. T_{NG}, T_C and T_H are surface temperatures at northern Greece, Crete, and Haifa, respectively.
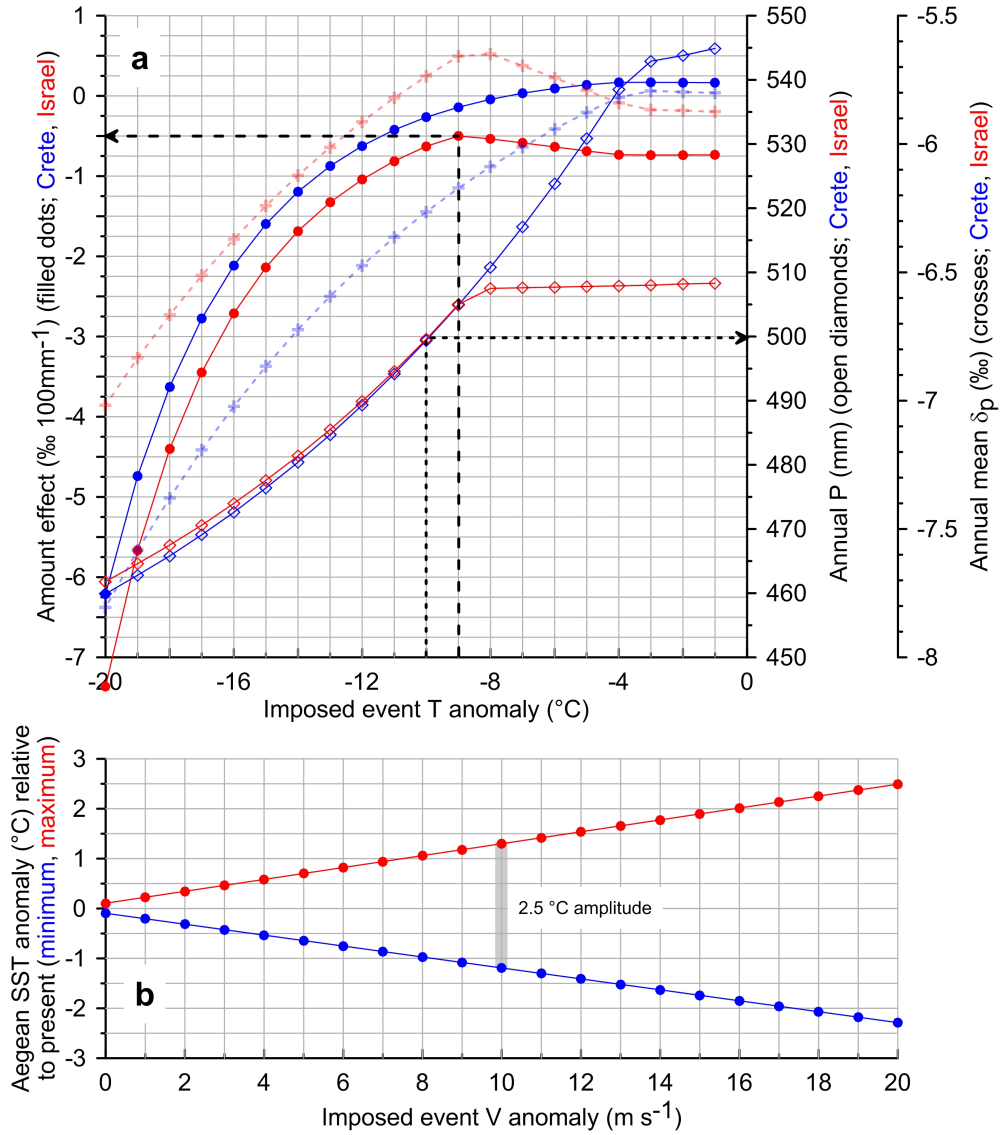
Figure 2. Model diagnostics. The main sensitivities are to the mean magnitude of cooling during the northerly cold air outbreak events, and to the wind speed anomalies during these events. (a) Dependence of several model parameters to the former; the model's emergent "amount effect" for precipitation/cave waters in Israel/the Levant is a strong diagnostic for setting the mean magnitude of cooling during the events. Arrows indicate the selected settings. (b) Dependence of Aegean sea-surface temperature on mean wind speed. The grey bar indicates the wind speed anomaly for which good agreement is reached between the modelled range of SST change and that in observations.
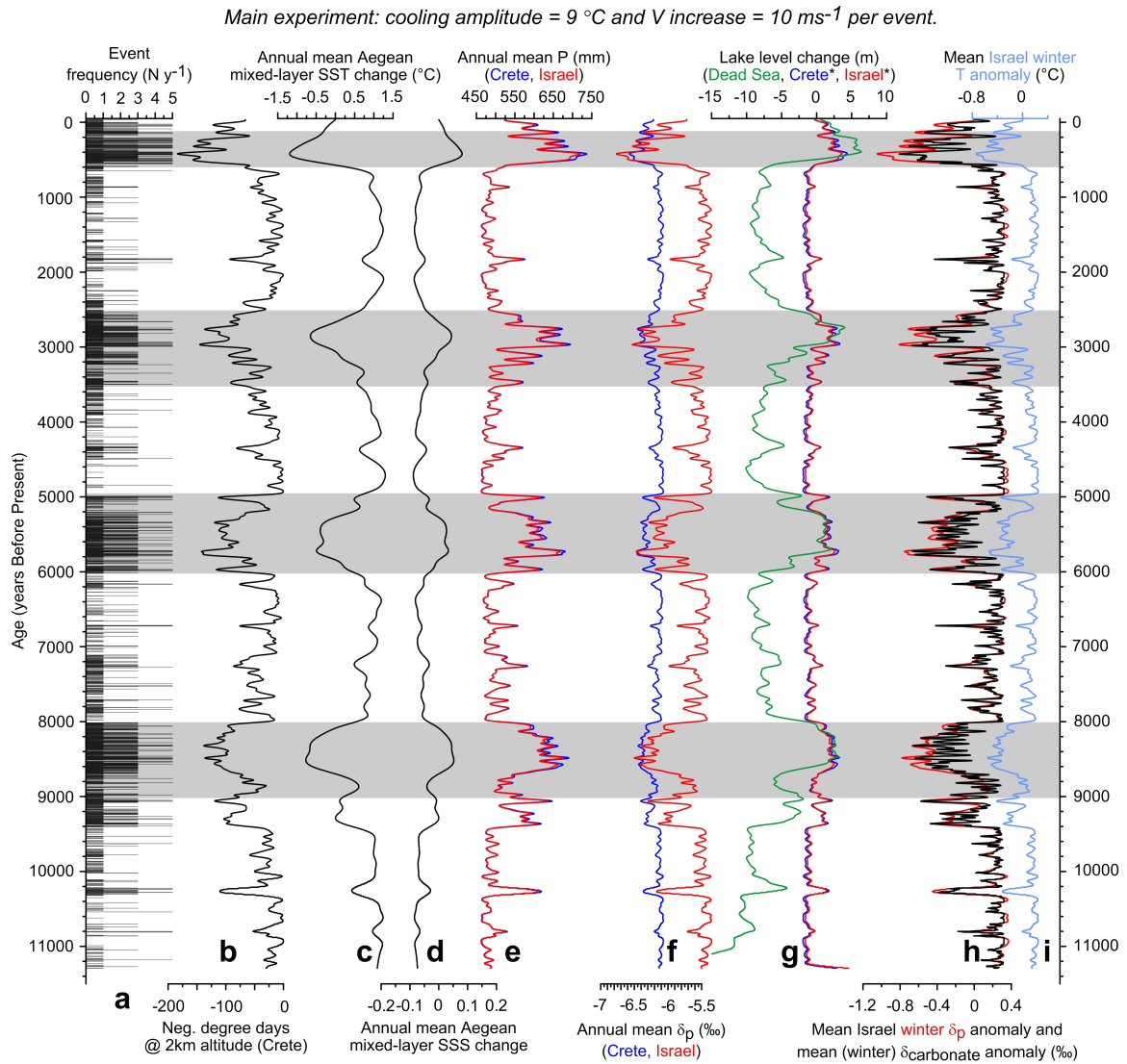
Figure 3. Time-series of results for the main model experiment. (*a*) Year type in terms of event frequency. (*b*) Negative degree days at 2 km altitude in Crete (more negative values indicate stronger snow/ice survival potential). (*c*) Aegean sea surface temperature. (*d*) Aegean sea surface salinity. (*e*) Annual mean *P* values for Crete (blue) and Israel (red). (*f*) Annual mean δ_P for Crete (blue) and Israel (red). (*g*) Lake level changes relative to the modern control value for hypothetical conical lakes in Crete (blue) and Israel (red), plus the simulated Dead-Sea-like basin (green). (*h*) Mean Israel winter δ_P anomaly (red) relative to the modern control value, and the mean winter carbonate $\delta^{18}O$ value for Israel (black), which are based on the δ_P anomalies and the mean winter temperature anomaly for Israel shown in (*i*). The temperature anomalies and thus carbonate $\delta^{18}O$ anomalies are values calculated at 0 m (sea-level) altitude. See text for the different smoothing factors used for different records, to best approximate potential resolutions in records of palaeo or historical data. The grey bars outline the main RCCs after (Mayewski et al., 2004).

24
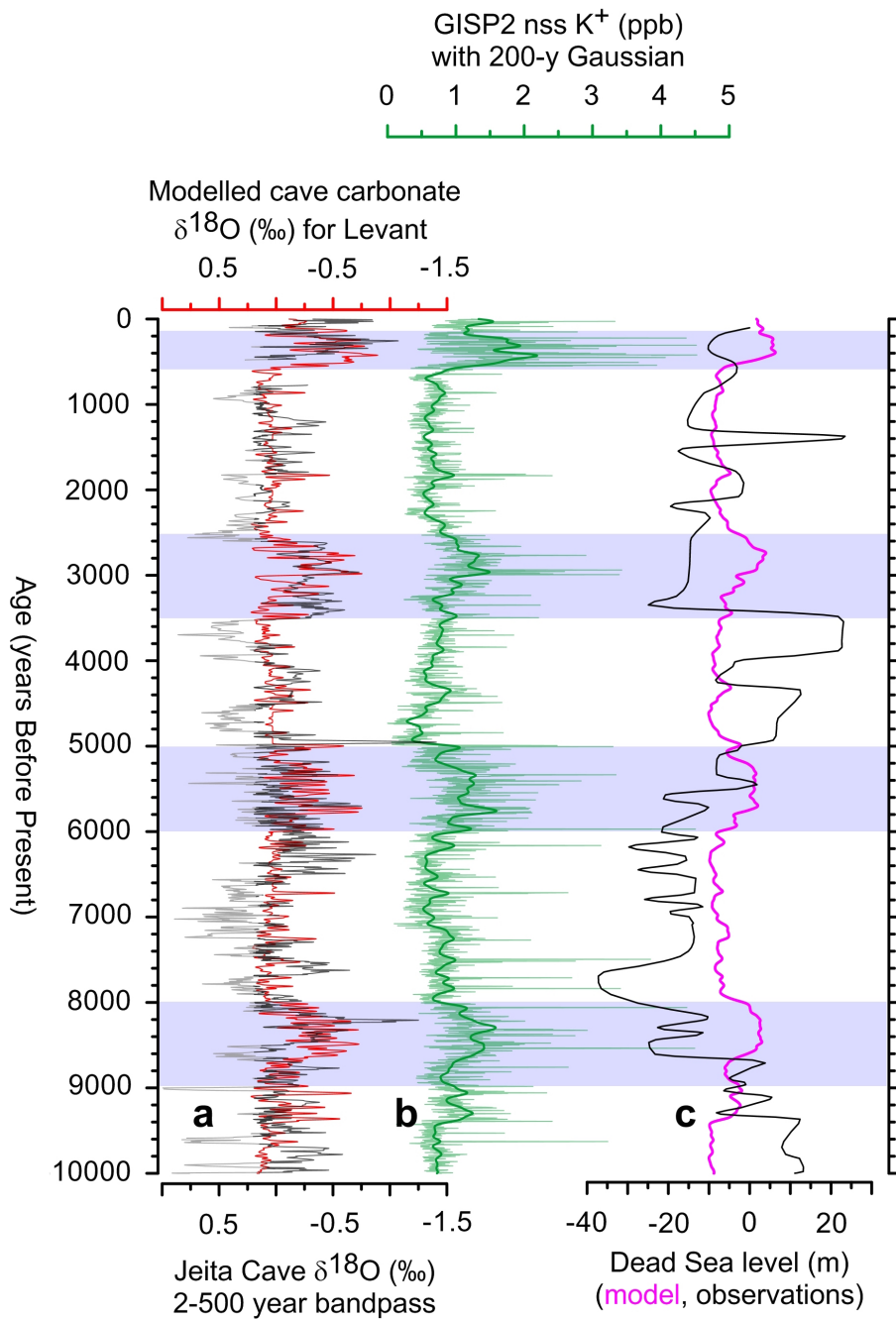
Figure 4. (*a*) Specific comparison of modelled cave-carbonate δ¹⁸O variations with the high-frequency (2-500 year bandpass) component of the Jeita Cave carbonate δ¹⁸O record from Lebanon (Cheng et al., 2015). In the Jeita Cave record, positive anomalies are shown in grey and negative anomalies in black. The modelled record was driven by the model's frequency of northerly outbreak events based on (*b*) the raw GISP2 K⁺ record (green, with 200-y Gaussian smoothing to show main trends). (*c*) Comparison between the model-generated record for a Dead Sea-like basin (magenta), with caveats discussed in the main text, and (black) the Dead Sea observations of Migowski et al. (2006).
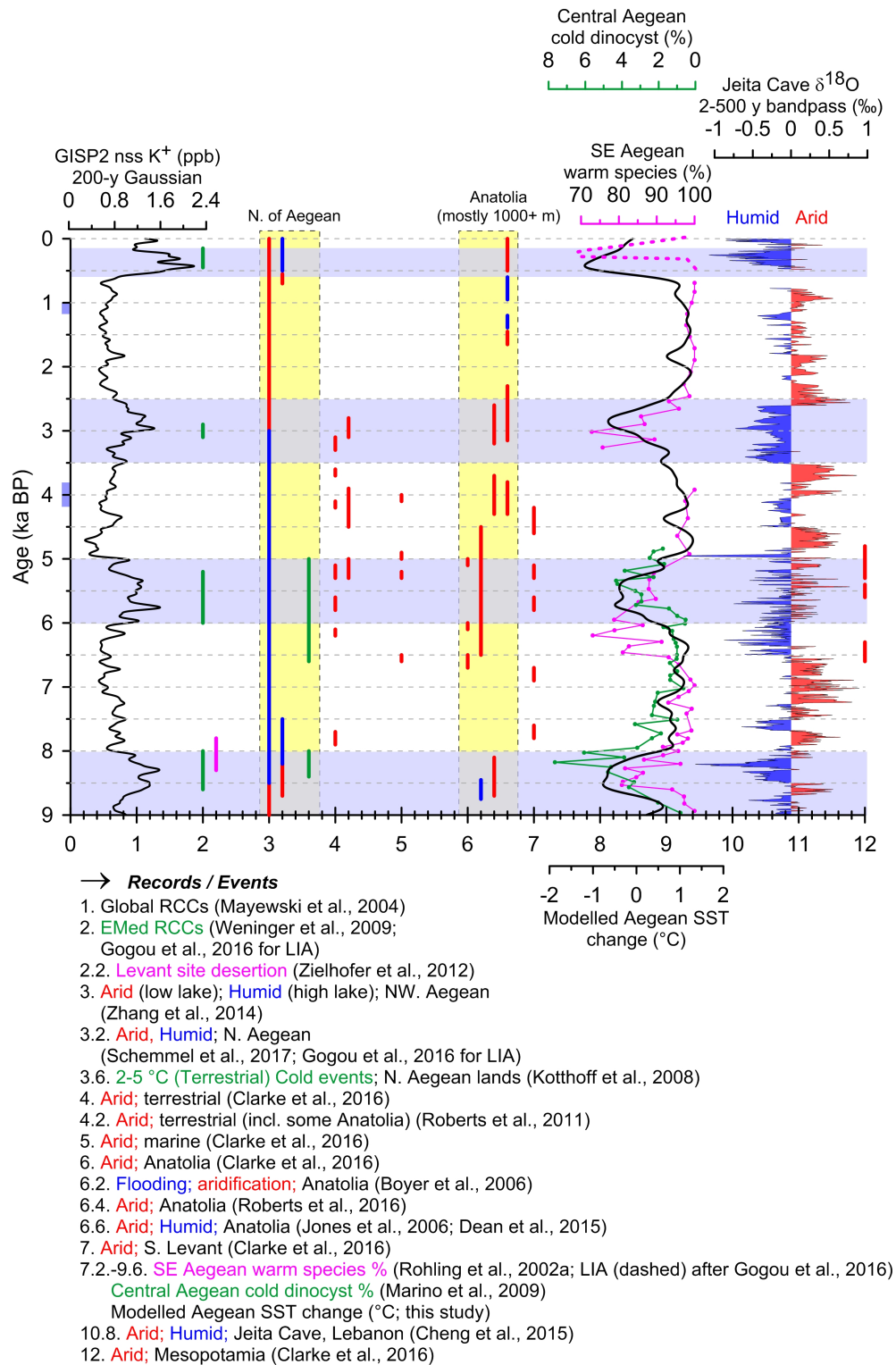
Figure 5. Comparison of signals as reported in the literature. Individual expressions in the study region are organised by numbered (x-axis) studies, organised roughly from the north to the south-southeast. The widespread Holocene RCCs described by Mayewski et al. (2004) are indicated with blue shading (small shaded blocks at about 4 and 1 ka BP indicated often-reported events that do not have clear expressions in the

The legend within the figure reads:

→ *Records / Events*
1. Global RCCs (Mayewski et al., 2004)
2. EMed RCCs (Weninger et al., 2009; Gogou et al., 2016 for LIA)
2.2. Levant site desertion (Zielhofer et al., 2012)
3. Arid (low lake); Humid (high lake); NW. Aegean (Zhang et al., 2014)
3.2. Arid, Humid; N. Aegean (Schemmel et al., 2017; Gogou et al., 2016 for LIA)
3.6. 2-5 °C (Terrestrial) Cold events; N. Aegean lands (Kotthoff et al., 2008)
4. Arid; terrestrial (Clarke et al., 2016)
4.2. Arid; terrestrial (incl. some Anatolia) (Roberts et al., 2011)
5. Arid; marine (Clarke et al., 2016)
6. Arid; Anatolia (Clarke et al., 2016)
6.2. Flooding; aridification; Anatolia (Boyer et al., 2006)
6.4. Arid; Anatolia (Roberts et al., 2016)
6.6. Arid; Humid; Anatolia (Jones et al., 2006; Dean et al., 2015)
7. Arid; S. Levant (Clarke et al., 2016)
7.2.-9.6. SE Aegean warm species % (Rohling et al., 2002a; LIA (dashed) after Gogou et al., 2016)
    Central Aegean cold dinocyst % (Marino et al., 2009)
    Modelled Aegean SST change (°C; this study)
10.8. Arid; Humid; Jeita Cave, Lebanon (Cheng et al., 2015)
12. Arid; Mesopotamia (Clarke et al., 2016)

GISP2 nssK$^+$ record). On the right-hand side are the well-defined Aegean SST trends and the high-frequency component of variability in Jeita Cave δ^{18}O.

990

References

Abu-Zied, R.H., Rohling, E.J., Jorissen, F.J., Fontanier, C., Casford, J.S.L., Cooke, S., 2008. Benthic foraminiferal response to changes in bottom-water oxygenation and organic carbon flux in the eastern Mediterranean during LGM to Recent times. Marine Micropaleontology 67, 46-68.

Alley, R.B., Mayewski, P.A., Sowers, T., Stuiver, M., Taylor, K.C., Clark, P.U., 1997. Holocene climatic instability: A prominent, widespread event 8200 yr ago. Geology 25, 483-486.

Alpert, P., Shafir, H., 1989. Mesog-Scale distribution of orographic precipitation: numerical study and comparison with precipitation derived from radar measurements. Journal of Applied Meteorology 28, 1105-1117.

Alpert, P., Neeman, B.U., and Shay-El, Y., 1990. Climatological analysis of Mediterranean cyclones using ECMWF data. Tellus 42A, 65-77.

Altaratz, O., Levin, Z., Yair, Y., 2001. Winter thunderstorms in israel: a study with lightning location systems and weather radar. Monthly Weather Review 129, 1259-1266.

Ammermann, A.J., Cavalli-Sforza, L.L., 1979. The wave of advance model for the spread of early farming. In C.Renfrew and K.L.Cooke (eds), Transformations: Mathematical Approaches to Culture Change, pp. 275-294. New York. Academic Press.

Anagnostopoulou, C., Tolika, K., Lazoglou, G., Maheras, P., 2017. The exceptionally cold January of 2017 over the Balkan Peninsula: a climatological and synoptic analysis. Atmosphere 8, 252, doi:10.3390/atmos8120252.

Anderson, D.G., Maasch, K.A., and Sandweiss, D.H. (eds.), 2007. Climate Change and Cultural Dynamics. A Global Perspective on Mid-Holocene Transitions. Academic Press. Elsevier.

Argiriou, A.A. , Lykoutis, S.P., 2005. Stable isotopes in rainfall over Greece: results of the 2000–2003 measurement campaign. In: Isotopic composition of precipitation in the Mediterranean Basin in relation to air circulation patterns and climate—Final report of a coordinated research project 2000–2004. IAEA-TECDOC-1453, pp. 83-97, IAEA, Austria.

Asouti E., Fuller, D.Q., 2013. A Contextual Approach to the Emergence of Agriculture in Southwest Asia. Current Anthropology 54, 299-345.

Barber, D.C., Dyke, A., Hillaire-Marcel, C., Jennings, A.E., Andrews, J.T., Kerwin, M.W., Bilodeau, G., McNeely, R., Southon, J., Morehead, M.D., Gagnon, J.M., 1999. Forcing of the cold event of 8,200 years ago by catastrophic drainage of Laurentide lakes. Nature 400, 344-348.

Bar-Matthews, M., Ayalon, A., 2011. Mid-Holocene climate variations revealed by high-resolution speleothem records from Soreq Cave, Israel and their correlation with cultural changes. Holocene 21, 163-171.

Bar-Matthews, M., Ayalon, A., Gilmour, M., Matthews, A., Hawkesworth, C.J., 2003. Sea-land oxygen isotopic relationships from planktonic foraminifera and speleothems in the Eastern Mediterranean region and their implication for paleorainfall during interglacial intervals. Geochimica et Cosmochimica Acta 67, 3181-3199.

Bar-Yosef, O.,1986. The Walls of Jericho: An Alternative Interpretation. Current Anthropology 27, 157-162.

1036 Ben Ami, Y., Altaratz, O., Yair, Y., Koren, I., 2015. Lightning characteristics over the
1037 eastern coast of the Mediterranean during different synoptic systems. Natural Hazards
1038 and Earth System Science 15, 2449-2459.

1039 Berger, J-F., Garyfalia, G., Guilaine, J., 2014. Vers une révision de la transition méso-
1040 néolithique sure le site de Sidari (Corfou, Grèce). Nouvelles données géoarcheologiques
1041 et radiocarbon, évaluation des processus pos-dépositionelles. In: Claire Manen, Thomas
1042 Perrin et Jean Guilaine (eds.), La Transition Néolithique en Méditerranée, Archives
1043 d'Écologie Préhistorique, Arles at Toulouse, pp. 209-228.

1044 Biehl, P.F., Nieuwenhuyse, O.P. (eds.), 2016. Climate and Cultural Change in Prehistoric
1045 Europe and the Near East. Suny Series. The Institute for European and Mediterranean
1046 Archaeology Distinguished Monograph Series.

1047 Borrell, F., Junno, A., Barceló, J.A., 2015. Synchronous Environmental and Cultural
1048 Change in the Emergence of Agricultural Economies 10,000 Years Ago in the Levant.
1049 PLoS ONE 10, doi:10.1371/journal.pone.0134810

1050 Bosmans, J.H.C., Drijfhout, S.S., Tuenter, E., Hilgen, F.J., Lourens, L.J., Rohling, E.J., 2015.
1051 Precession and obliquity forcing of the freshwater budget over the
1052 Mediterranean. Quaternary Science Reviews 123, 16–30.

1053 Boyer, P., Roberts, N., Baird, D., 2006. Holocene environment and settlement on the
1054 Çarşamba alluvial fan, south-central Turkey: integrating geoarchaeology and
1055 archaeological field survey. Geoarchaeology 21, 675-698.

1056 Budja, M. 2007. The 8200 calBP 'climate event' and the process of neolithisation in
1057 south-eastern Europe. Documenta Praehistorica 34, 191-201.

1058 Budja, M., 2015. Archaeology and rapid climate changes: from the collapse concept to a
1059 panarchy interpretive model. Documenta Praehistorica XLII, 171-184.

1060 Cacho, I., Grimalt, J.O., Canals, M., Sbaffi, L., Shackleton, N.J., Schonfeld, J., Zahn, R., 2001.
1061 Variability of the western Mediterranean Sea surface temperature during the last
1062 25,000 years and its connection with the Northern Hemisphere climatic changes.
1063 Paleoceanography 16, 40-52.

1064 Cacho, I., Grimalt, J.O., Pelejero, C., Canals, M., Sierro, F.J., Flores, J.A., Shackleton, N.,
1065 1999. Dansgaard-Oeschger and heinrich event imprints in Alboran Sea
1066 paleotemperatures. Paleoceanography 14, 698-705.

1067 Cacho, I., Grimalt, J.O., Sierro, F.J., Shackleton, N., Canals, M., 2000. Evidence for enhanced
1068 Mediterranean thermohaline circulation during rapid climatic coolings. Earth and
1069 Planetary Science Letters 183, 417-429.

1070 Carletti, C., Sciurpi, F., Pierangioli, L., 2014. The energy upgrading of existing buildings:
1071 window and shading device typologies for energy efficiency refurbishment.
1072 Sustainability 6, 5354-5377.

1073 Casford, J.S.L., Abu-Zied, R., Rohling, E.J., Cooke, S., Boessenkool, K.P., Brinkhuis, H., De
1074 Vries, C., Wefer, G., Geraga, M., Papatheodorou, G., Croudace, I., Thomson, J., Wells, N.C.,
1075 Lykousis, V., 2001. Mediterranean climate variability during the Holocene.
1076 Mediterranean Marine Science 2, 45-55.

1077 Casford, J.S.L., Rohling, E.J., Abu-Zied, R.H., Fontanier, C., Jorissen, F.J., Leng, M.J.,
1078 Schmiedl, G., Thomson, J., 2003. A dynamic concept for eastern Mediterranean
1079 circulation and oxygenation during sapropel formation. Palaeogeography
1080 Palaeoclimatology Palaeoecology 190, 103-119.

1081 Cheng, H., Sinha, A., Verheyden, S., Nader, F.H., Li, X.L., Zhang, P.Z., Yin, J.J., Yi, L., Peng,
1082 Y.B., Rao, Z.G., Ning, Y.F., Edwards, R.L., 2015. The climate variability in northern Levant
1083 over the past 20,000 years. Geophysical Research Letters 42, 8641-8650.

1084 Clare, L., 2016. Culture Change and Continuity in the Eastern Mediterranean during
1085 Rapid Climate Change. Assessing the vulnerability of Late Neolithic communities to a
1086 "Little Ice Age" in the seventh millennium cal B.C. *Kölner Studien zur Prähistorischen*
1087 *Archäologie 7*. Verlag Marie Leidorf.

1088 Clare, L., Rohling, E.J., Weninger, B., Hilpert, J., 2008. Warfare in Late Neolithic/Early
1089 Chalcolithic Pisidia, southwestern Turkey. Climate induced social unrest in the late 7th
1090 millennium calBC, In: Budja, M. (Ed.), Documenta Praehistorica XXXV, 65-92.

1091 Clarke, J., Brooks, N., Banning, E.B., Bar-Matthews, M., Campbell, S., Clare, L., Cremaschi,
1092 M., di Lernia, S., Drake, N., Gallinaro, M., Manning, S., Nicoll, K., Philip, G., Rosen, S.,
1093 Schoop, U.D., Tafuri, M.A., Weninger, B., Zerboni, A., 2016. Climatic changes and social
1094 transformations in the Near East and North Africa during the 'long' 4th millennium BC:
1095 A comparative study of environmental and archaeological evidence. Quaternary Science
1096 Reviews 136, 96-121.

1097 Climatedata (last visited 1-03-2018). https://www.climatedata.eu/

1098 Climatemps.alexandroupoli (last visited 1-03-2018).
1099 http://www.alexandroupoli.climatemps.com

1100 Climatemps.crete (last visited 1-03-2018). http://www.crete.climatemps.com

1101 Climatemps.haifa (last visited 1-03-2018). http://www.haifa.climatemps.com

1102 Climatemps.plovdiv (last visited 1-03-2018). http://www.plovdiv.climatemps.com

1103 Cline, E.H., 2014. *1177 B.C.: the year civilization collapsed*. Princeton University Press,
1104 Princeton U.S.A, p. 237. ISBN978-0691-14089-6.

1105 CNN WEATHER, 2001. Posted: December 19, 8:53 AM EST (1353 GMT). http://archives.
1106 cnn.com/2001/WEATHER/12/19/greece.romania/index. html

1107 Constantin, S., Bojar, A. V., Lauritzen, S. E., and Lundberg, J., 2007. Holocene and Late
1108 Pleistocene climate in the sub-Mediterranean continental environment: A speleothem
1109 record from Poleva Cave (Southern Carpathians, Romania). Palaeogeography
1110 Palaeoclimatology Palaeoecology 243, 322-338.

1111 Coulter, D., 2012. Europe hammered by winter, is North America next?
1112 https://science.nasa.gov/science-news/science-at-nasa/2012/16feb_deepfreeze

1113 Dailymail. http://www.dailymail.co.uk/news/article-2260223/Jerusalem-hit-worst-
1114 snowstorm-TWENTY-YEARS-inches-falls-Holy-City-closing-roads-schools.html

1115 Dayan, U., Lifshitz-Goldreich, B., Pick, K., 2002. Spatial and structural variation of the
1116 atmospheric boundary layer during summer in israel—profiler and rawinsonde
1117 measurements. Journal of Applied Meteorology 41, 447-457.

1118 Dayan, U., Ricaud, P., Zbinden, R., Dulac,F., 2017. Atmospheric pollution over the eastern
1119 Mediterranean during summer – a review. Atmospheric Chemistry and Physics 17,
1120 13233-13263.

1121 Dayan, U., Rodnizki, J., 1999. The temporal behavior of the atmospheric boundary layer
1122 in Israel. Journal of Applied Meteorology 38, 830-836.

1123 Dean, J.R., Jones, M.D., Leng, M.J., Sloane, H.J., Roberts, C.N., Woodbridge, J., Swann, G.E.A.,
1124 Metcalfe, S.E., Eastwood, W.J., Yigitbasioglu, H., 2013. Palaeo-seasonality of the last two

millennia reconstructed from the oxygen isotope composition of carbonates and diatom silica from Nar Golu, central Turkey. Quaternary Science Reviews 66, 35-44.

Dean, J.R. Jones, M.D., Leng, M.J., Noble, S.R., Metcalfe, S.E., Sloane, H.J., Sahy, D., Eastwood, W.J., Roberts, C.N., 2015. Eastern Mediterranean hydroclimate over the late glacial and Holocene, reconstructed from the sediments of Nar lake, central Turkey, using stable isotopes and carbonate mineralogy. Quaternary Science Reviews 124, 162-174.

Dirican, A., Ünal, S., Acar, Y., Demircan, M., 2005. The temporal and seasonal variation of H-2 and O-18 in atmospheric water vapour and precipitation from Ankara, Turkey in relation to air mass trajectories at Mediterranean basin. In: Isotopic composition of precipitation in the Mediterranean Basin in relation to air circulation patterns and climate—Final report of a coordinated research project 2000–2004. IAEA-TECDOC-1453, pp. 191-214, IAEA, Austria.

Dotsika, E., Lykoudis, S., Poutoukis, D., 2010. Spatial distribution of the isotopic composition of precipitation and spring water in Greece. Global and Planetary Change 71, 141-149.

Feurdean, Angelica, Stefan Klotz, Volker Mosbrugger, and Barbara Wohlfarth, 2008. Pollen-based quantitative reconstructions of Holocene climate variability in NW Romania, Palaeoclimatology Palaeogeography Palaeoecology 260, 494-504.

Fiedel, S.J., Anthony, D.W., 2003. Deerslayers, pathfinders and Icemen. Origins of the European Neolithic as seen from the frontier. In: Rockman, M., Steele, J. (eds.), Colonization Unfamiliar Landscapes: the Archaeology of Adaptation. Routledge, pp. 144-168.

Floodlist. http://floodlist.com/asia/heavy-rainfall-floods-israel

Frigola, J., Moreno, A., Cacho, I., Canals, M., Sierro, F.J., Flores, J.A., Grimalt, J.O., Hodell, D.A., Curtis, J.H., 2007. Holocene climate variability in the western Mediterranean region from a deepwater sediment record. Paleoceanography 22, PA2209, 10.1029/2006PA001307.

Fuller, D.Q., Asouti, E., Purugganan, M.D., 2012. Cultivation as slow evolutionary entanglement: Comparative data on rate and sequence of domestication. Veg Hist Archaeobot 21,131–145.

Galvin, J., Black, I., Priestley, D., 2011. Mesoscale weather features over the Mediterranean: Part 1. Weather 66, 72-78.

Ganot, M., Yair, Y., Price, C., Ziv, B., Sherez, Y., Greenberg, E., Devir, A., Yaniv, R., 2007. First detection of transient luminous events associated with winter thunderstorms in the eastern Mediterranean. Geophysical Research Letters 34, L12801, doi:10.1029/2007GL029258.

Gat, J.R., 1996. Oxygen and hydrogen isotopes in the hydrological cycle. Annual Review of Earth and Planetary Sciences 24, 225-262.

Gat, J.R., Ben-Mair, R., Yam, R., Yakir, D., Wernli, H., 2005. The isotope composition of atmospheric waters in Israel's coastal plain. In: Isotopic composition of precipitation in the Mediterranean Basin in relation to air circulation patterns and climate—Final report of a coordinated research project 2000–2004. IAEA-TECDOC-1453, pp. 99-114, IAEA, Austria.

1169 Gebel , H.G.K., 2009. The Intricacy of Neolithic Rubble Layers. The Ba'ja, Basta, and 'Ain
1170 Rahub evidence. In: (eds. Gebel, H.G.K. an Rollefson, G.O.). Special Issue on Rubble
1171 Layers and Rapid Climate Change, Neo-Lithics 1/09, 33-46.

1172 Gkinis, V., Simonsen, S.B., Buchardt, S.L., White, J.W.C., Vinther, B.M., 2014. Water isotope
1173 diffusion rates from the NorthGRIP ice core for the last 16,000 years – Glaciological and
1174 paleoclimatic implications. Earth and Planetary Science Letters 405, 132-141.

1175 Gogou, A., Triantaphyllou, M., Xoplaki, E., Izdebski, A., Parinos, C., Dimiza, M.,
1176 Bouloubassi, I., Luterbacher, J., Kouli, K., Martrat, B., Toreti, A., Fleitmann, D., Rousakis,
1177 G., Kaberi, H., Athanasiou, M., Lykousis, V., 2016. Climate variability and socio-
1178 environmental changes in the northern Aegean (NE Mediterranean) during the last
1179 1500 years. Quaternary Science Reviews 136, 209-228.

1180 Gonfiantini, R., 1986. Environmental isotopes in lake studies. In: Fritz, P., Fontes, J.C.,
1181 Handbook of environmental isotope geochemistry, pp. 113-168, Elsevier, New York.

1182 Grunewald, K., Scheithauer, J., 2010. Europe's southernmost glaciers: response and
1183 adaptation to climate change. Journal of Glaciology 56, 129-142.

1184 Guilaine J., 2001. La diffusion de l'agriculture en Europe: une hypothese arythmique.
1185 Zephyrus 53, 267–272.

1186 Heun, M., Abbo, S., Kev-Yadun, Gopher, A., 2012. A critical review of the protracted
1187 domestication model for Near-Eastern founder crops: linear regression, log-distance
1188 gene flow, archaeological and archaeobotanical evidende. Journal of Experimental
1189 Botany 63, 4333-4341.

1190 Hillman, G.C., Davies, M.S., 1990. Domestication rates in wild type wheats and barley
1191 under primitive cultivation. Biological Journal of the Linnean Society 39, 39–78.

1192 Hoefs, J., 1996. Stable isotope geochemistry: fourth completely revised, updated, and
1193 enlarged edition, 201 pp. Springer-Verlag, Berlin.

1194 Honne, B.I., Heun, M., 2009. On the domestication genetics of self-fertilizing plants.
1195 Vegetation History and Archaeobotany 18, 269-272.

1196 Horejs, B., Milić, B., Ostmann, F., Thanheiser, U., Weninger, B., Galik, A., 2015. The Aegean
1197 in the Early 7th Millennium BC: Maritime Networks and Colonization. Journal of World
1198 Prehistory 28, 289-330.

1199 Hughes, P.D., 2014. Little Ice Age glaciers in the Mediterranean mountains,
1200 Méditerranée, 122, 63-97.

1201 Incarbona, A., Martrat, B., Mortyn, P.G., Sprovieri, M., Ziveri, P., Gogou, A., Jordà, G.,
1202 Luterbacher, J., Lagnone, L., Marino, G., Rodríguez-Sanz, L., Triantaphyllou, M., Di
1203 Stefano, E., Grimalt, J.O., Tranchida, G., Sprovieri, R., Mazzola, S., 2016. Mediterranean
1204 circulation perturbations over the last five centuries: Relevance to past Eastern
1205 Mediterranean Transient-type events. Scientific Reports 6: 29623, DOI:
1206 10.1038/srep29623, 1-10.

1207 Israelnationalnews. http://www.israelnationalnews.com/News/News.aspx/187927

1208 Jones, M.D., Roberts, C.N., Leng, M.J., Türkeş, M., 2006. A high-resolution late Holocene
1209 lake isotope record from Turkey and links to North Atlantic and monsoon climate.
1210 Geology 34, 361-364.

1211 Josey, S.A., Somot, S., Tsimplis, M., 2011. Impacts of atmospheric modes of variability on
1212 Mediterranean Sea surface heat exchange. Journal of Geophysical Research-Oceans 116,
1213 C02032, doi:10.1029/2010JC006685.

Kagan, E.J., Langgut, D., Boaretto, E., Neumann, F.H., Stein, M., 2015. Dead Sea levels during the Bronze and Iron Ages. Radiocarbon 57, 237-252.

Kaniewski, D., Paulissen,E., Van Campo, E., Weiss, H., Otto, T., Bretschneider, T., Van Lerberghe, K., 2010. Late second–early first millennium BC abrupt climate changes in coastal Syria and their possible significance for the history of the Eastern Mediterranean. Quaternary Research 74, 207-215

Kaniewski, D., Marriner, N., Ilan, D., Morhange, C., Thareani, V., Van Campo, E., 2017. Climate change and water management in the biblical city of Dan. Science Advances, 3: e1700954, 1-8.

Kotthoff, U., Pross, U., Müller, U.C., Peyron, O., Schmiedl, G., Schultz, H., Bordon, A., 2008. Climate dynamics in the borderlands of the Aegean Sea during formation of sapropel S1 deduced from a marine pollen record. Quaternary Science Reviews 27, 832-845.

Krauß, R., Marinova, E., De Brue, H., Weninger, B., 2017. The rapid spread of early farming from the Aegean into the Balkans via the Sub-Mediterranean-Aegean Vegetation Zone. Quaternary International xxx, 1-8 (*in press*). doi.org/10.1016/j.quaint.2017.01.019

Krichak, S. O., Alpert, P., and Dayan, M., 2004. The role of atmospheric processes associated with Hurricane Olga in the December 2001 Floods in Israel. Journal of Hydrometeorology 5, 1259–1270.

Kuhlemann, J., Rohling, E.J., Kumrei, I., Kubik, P., Ivy-Ochs, S., Kucera, M., 2008. Regional synthesis of Mediterranean atmospheric circulation during the Last Glacial Maximum. Science 321, 1338-1340.

Kuhnt, T., Schmiedl, G., Ehrmann, W., Hamann, Y., Hemleben, C., 2007. Deep-sea ecosystem variability of the Aegean Sea during the past 22 kyr as revealed by Benthic Foraminifera. Marine Micropaleontology 64, 141-162.

Kuper, R. and Kröpelin, S., 2006. Climate-Controlled Holocene Occupation in the Sahara: Motor of Africa's Evolution. Science 313, 803-807.

Leaman, K.D., Schott, F.A., 1991. Hydrographic structure of the convection regime in the Gulf of Lions: Winter 1987. Journal of Physical Oceanography 21, 575-598.

Lespez, L., Tsirtsoni, Z., Darcque, P., Koukouli-Chryssanthraki, H., Malamidou, D., Treuil, R., Oberlin, C. , 2013. The lowest levels at Dikili Tash, northern Greece: a missing link in the Early Neolithic of Europe. Antiquity 87, 30-45.

Linstädter, J., Broich, M., Weninger, B., 2016. Defining the Early Neolithic of the Eastern Rif, Morocco - Spatial distribution, chronological framework and impact of environmental changes. Quaternary International XXX, 1-11.

Lionello, P., Malanotte-Rizzoli, P., Boscolo, R., 2006. *Mediterranean climate variability, Vol. 4.*, Elsevier, 438 pp., ISBN9780444521705

Litt, T., Ohlwein, C., Neumann, F.H., Hense, A., Stein, M., 2012. Holocene climate variations in the Levant from the Dead Sae pollen record. Quaternary Science Reviews 49, 95-105.

Lolis, C.J., Bartzokas, A., Katsoulis, B.D., 2002. Spatial and temporal 850 hPA air temperature and sea-surface temperature covariances in the Mediterranean region and their connection to atmospheric circulation. International Journal of Climatology 22, 663-676.

1258 Luterbacher, J., Xoplaki, E., Casty, C., Wanner, H., Pauling, A., Küttel, M., Ruthishauser, T.,
1259 Brönnimann, S., Fischer, E., Fleitmann, D., González-Rouco, F.J., García-Herrera, R.,
1260 Barriendos, M., Rodrigo, F., Gonzalez-Hidalgo, J.C., Angel Saz, M., Gimeno, L., Ribera, P.,
1261 Brunet, M., Paeth, H., Rimbu, N., Felis, T., Jacobeit, J., Dünkeloh, A., Zorita, E., Guiot, J.,
1262 Türkes, M., Joao Alcoforado, M., Trigo, R., Wheeler, D., Tett, S., Mann, M.E., Touchan, R.,
1263 Shindell, D., Silenzi, S., Montagna, P., Camuffo, D., Meriotti, A., Nanni, T., Brunetti, M.,
1264 Maugeri, M., Zerefos, C., De Zolt, S., Lionello, P., 2006. In: Lionello, P., Malanotte-Rizzoli,
1265 P., Boscolo, R., Eds. The Mediterranean Climate: An Overview of the Main Characteristics
1266 and Issues (Elsevier, Amsterdam, 2006), pp. 27-148.

1267 Maheras, P., Xoplaki, E., Davies, T., Martin-Vide, J., Bariendos, M., Alcoforado, M.J., 1999.
1268 Warm and cold monthly anomalies across the Mediterranean basin and their
1269 relationship with circulation; 1860-1990. International Journal of Climatology 19, 1697-
1270 1715.

1271 Majoube, M., 1971. Fractionnement en oxygène 18 et deuterium entre l'eau et sa vapeur.
1272 Journal de Chimie Physique 10, 1423-1436.

1273 Mangini, A., Verdes, P., Spotl, C., Scholz, D., Vollweiler, N., Kromer, B., 2007. Persistent
1274 influence of the North Atlantic hydrography on central European winter temperature
1275 during the last 9000 years. Geophysical Research Letters 34, L02704,
1276 doi:10.1029/2006GL028600.

1277 Marino, G., Rohling, E.J., Sangiorgi, F., Hayes, A., Casford, J.L., Lotter, A.F., Kucera, M.,
1278 Brinkhuis, H., 2009. Early and middle Holocene in the Aegean Sea: interplay between
1279 high and low latitude climate variability. Quaternary Science Reviews 28, 3246-3262.

1280 Mariolopoulos, E.G., 1961. An outline of the climate of Greece. Publications of the
1281 Meteorological Institute of the University of Athens 6, 51 pp.

1282 Mayewski, P.A., Meeker, L.D., Twickler, M.S., Whitlow, S., Yang, Q.Z., Lyons, W.B.,
1283 Prentice, M., 1997. Major features and forcing of high-latitude northern hemisphere
1284 atmospheric circulation using a 110,000-year-long glaciochemical series. Journal of
1285 Geophysical Research-Oceans 102, 26345-26366.

1286 Mayewski, P.A., Rohling, E.E., Stager, J.C., Karlen, W., Maasch, K.A., Meeker, L.D.,
1287 Meyerson, E.A., Gasse, F., van Kreveld, S., Holmgren, K., Lee-Thorp, J., Rosqvist, G., Rack,
1288 F., Staubwasser, M., Schneider, R.R., Steig, E.J., 2004. Holocene climate variability.
1289 Quaternary Research 62, 243-255.

1290 Meeker, L.D., Mayewski, P.A., 2002. A 1400-year high-resolution record of atmospheric
1291 circulation over the North Atlantic and Asia. Holocene 12, 257-266.

1292 Mercone, D., Thomson, J., Abu-Zied, R.H., Croudace, I.W., Rohling, E.J., 2001. High-
1293 resolution geochemical and micropalaeontological profiling of the most recent eastern
1294 Mediterranean sapropel. Marine Geology 177, 25-44.

1295 Merlivat, L., Jouzel, J. 1979. Global climatic interpretation pf the deuterium-oxygen 18
1296 relationship for precipitation. Journal of Geophysical Research 84, 5029-5033.

1297 Migowski, C., Stein, M., Prasad, S., Negendank, J.F.W., Agnon, A, 2006. Holocene climate
1298 variability and cultural evolution in the Near East from the Dead Sea sedimentary
1299 record. Quaternary Research 66, 421-431.

1300 Moreno-Chamarro, E., Zanchettin, D., Lohmann, K., Luterbacher, J., Junclaus, J.H., 2017.
1301 Winter amplification of the European Little Ice Age cooling by the subpolar gyre.
1302 Scientific Reports 7: 9981, DOI:10.1038/s41598-017-07969-0, 1-8.

Muschitiello, F., Schwark, L., Wolfarth, B., Sturm, C., Hammarlund, D., 2013. New evidence of Holocene atmospheric circulation dynamics based on lake sediments from southern Sweden: a link to the Siberian High. Quaternary Science Reviews 77, 113-124.

Nieuwenhuyse, O., 2017. Globalizing the Halaf. In: Tamar Hodos (ed.). The Routledge Handbook of Archaeology and Globalization. Routledge. London and New York. 839-854.

O'Brien, S.R., Mayewski, P.A., Meeker, L.D., Meese, D.A., Twickler, M.S., Whitlow, S.I., 1995. Complexity of Holocene climate as reconstructed from a Greenland ice core. Science 270, 1962-1964.

Panagiotopoulos F, Shagedanova M, Hannachi A, Stephenson D., 2005. Observed trends and teleconnections of the Siberian High: a recently declining center of action. Journal of Climate 18, 1411-1422.

Peyron, O., Goring, S., Dormoy, I., Kotthoff, U., Pross, J., de Beaulieu, J.L., Drescher-Schneider, R., Vanniere, B., Magny, M., 2011. Holocene seasonality changes in the central Mediterranean region reconstructed from the pollen sequences of Lake Accesa (Italy) and Tenaghi Philippon (Greece). Holocene 21, 131-146.

Plicht, J. van der, Akkermans, P., Nieuwenhuyse, O., Kaneda, A., Russell, A., 2011. Tell Sabi Abyad, Syria: Radiocarbon Chronology, Cultural Change, and the 8.2 Ka Event. Radiocarbon 53, 229-243.

Poulos, S.E., Drakopoulos, P.G., Collins, M.B., 1997. Seasonal variability in sea surface oceanographic conditions in the Aegean Sea (Eastern Mediterranean): an overview. Journal of Marine Systems 13, 225-244.

Pross, J., Kotthoff, U., Muller, U.C., Peyron, O., Dormoy, I., Schmiedl, G., Kalaitzidis, S., Smith, A.M., 2009. Massive perturbation in terrestrial ecosystems of the Eastern Mediterranean region associated with the 8.2 kyr BP climatic event. Geology 37, 887-890.

Revel, M., Ducassou, E., Frousset, F.E., Bernasconi, S.M., Migeon, S., Revillon, S., Mascle, J., Murat, A., Zaragosi, S., Bosch, D., 2010. 100,000 Years of African monsoon variability recorded in sediments of the Nile margin. Quaternary Science Reviews 29, 1342-1362.

Roberts, N., Allcock, S.L., Arnaud, F., Dean, J.R., Eastwood, W.J., Jones, M.D., Leng, M.J., Metcalfe, S.E., Malet, E., Woodbridge, J., Yigitbasioglu, H., 2016. A tale of two lakes: a multi-proxy comparison of Lateglacial and Holocene environmental change in Cappadocia, Turkey. Journal of Quaternary Science 31, 348-362.

Roberts, N., Brayshaw, D., Kuzucuoglu, C., Perez, R., Sadori, L., 2011. The mid-Holocene climatic transition in the Mediterranean: Causes and consequences. Holocene 21, 3-13.

Roether, W., Manca, B.B., Klein, B., Bregant, D., Georgopoulos, D., Beitzel, V., Kovacevic, V., Luchetta, A., 1996. Recent changes in eastern Mediterranean deep waters. Science 271, 333-335.

Rohling, E.J., 1999. Environmental control on Mediterranean salinity and δ^{18}O. Paleoceanography 14, 706-715.

Rohling, E.J., 2013. Quantitative assessment of glacial fluctuations in the level of Lake Lisan, Dead Sea rift. Quaternary Science Reviews 70, 63-72.

Rohling, E.J., 2016. Of lakes and fields: A framework for reconciling palaeoclimatic drought inferences with archaeological impacts. Journal of Archaeological Science 73, 17-24.

Rohling, E.J., Casford, J., Abu-Zied, R., Cooke, S., Mercone, D., Thomson, J., Croudace, I., Jorissen, F.J., Brinkhuis, H., Kallmeyer, J., Wefer, G., 2002a. Rapid Holocene climate changes in the eastern Mediterranean. In Hassan, F. (ed.) *Droughts, Food and Culture: Ecological Change and Food Security in Africa's Later Prehistory*, Kluwer Academic/Plenum Publishers, London, pp. 35-46.

Rohling, E.J., Hayes, A., Mayewski, P.A., Kucera, M., 2009. Holocene climate variability in the eastern Mediterranean, and the End of the Bronze Age. In: Bachhuber, C. and Roberts, R.G. (eds.) *Forces of Transformation: The End of the Bronze Age in the Mediterranean*. BANEA Publication Series 1, Oxbow Books, Oxford, ISBN-13: 978-1-84217-332-9, pp. 2–5.

Rohling, E.J., Jorissen, F.J., DeStigter, H.C., 1997. 200 year interruption of Holocene sapropel formation in the Adriatic Sea. Journal of Micropalaeontology 16, 97-108.

Rohling, E.J., Marino, G., Grant, K.M., 2015. Mediterranean climate and oceanography, and the periodic development of anoxic events (sapropels). Earth Science Reviews 143, 62–97.

Rohling, E.J., Mayewski, P.A., Abu-Zied, R.H., Casford, J.S.L., Hayes, A., 2002b. Holocene atmosphere-ocean interactions: records from Greenland and the Aegean Sea. Climate Dynamics 18, 587-593.

Rohling, E.J., Mayewski, P.A., Challenor, P., 2003. On the timing and mechanism of millennial-scale climate variability during the last glacial cycle. Climate Dynamics 20, 257-267.

Rohling, E.J., Pälike, H., 2005. Centennial-scale climate cooling with a sudden cold event around 8,200 years ago. Nature 434, 975-979.

Rohling, E.J., Sprovieri, M., Cane, T., Casford, J.S.L., Cooke, S., Bouloubassi, I., Emeis, K.C., Schiebel, R., Rogerson, M., Hayes, A., Jorissen, F.J., Kroon, D., 2004. Reconstructing past planktic foraminiferal habitats using stable isotope data: a case history for Mediterranean sapropel S5. Marine Micropaleontology 50, 89-123.

Rollefson, G.O., 2009. Slippery Slope: The Late Neolithic Rubble Layer in the Southern Levant. In: (eds. Gebel, H.G.K. an Rollefson, G.O.). Special Issue on Rubble Layers and Rapid Climate Change, Neo-Lithics 1/09, 12-18.

Rozanski, K., Araguas-Araguas, L, Gonfiantini, R., 1993. Isotopic patterns in modern global precipitation. In: Swart, P.K., Climate change in continental isotopical records. Geophysical Monograph Series 78, pp.1-36. American Geophysical Union, Washington D.C.

Saaroni, H., Bitan, A., Alpert, P., Ziv, B., 1996. Continental polar outbreaks into the Levant and eastern Mediterranean. International Journal of Climatology 16, 1175-1191.

Saaroni, H., Halfon, N., Ziv, B., Alpert, P., and Kutiel, H., 2010. Links between the rainfall regime in Israel and location and intensity of Cyprus lows. International Journal of Climatology 30, 1014-1025.

Schemmel, F., Niedermeyer, E.M., Koutsodendris, A., Pross, J., Fiebig, J., Mulch, A., 2017. Paleohydrological changes in the Eastern Mediterranean region during the early to mid-Holocene recorded in plant wax n-alkane distributions and delta C-13(TOC) - New data from Tenaghi Philippon, NE Greece. Organic Geochemistry 110, 100-109.

Schemmel, F., Niedermeyer, E.M., Schwab, V.F., Gleixner, G., Pross, J., Mulch, A., 2016. Plant wax delta D values record changing Eastern Mediterranean atmospheric

circulation patterns during the 8.2 kyr BP climatic event. Quaternary Science Reviews 133, 96-107.

Schemmel, F., Niedermeyer, E.M., Koutsodendris, A., Pross, J., Fiebig, J., Mulch, A., 2017. Paleohydrological changes in the Eastern Mediterranean region during the early to mid-Holocene recorded in plant wax n-alkane distributions and $\delta^{13}C_{TOC}$ – New data from Tenaghi Philippon, NE Greece. Organic Geochemistry 110, 100-109.

Schmiedl, G., Kuhnt, T., Ehrmann, W., Emeis, K.-C., Hamann, Y., Kotthoff, U., Dulski, O., Pross, J., 2010. Climatic Forcing of eastern Mediterranean deep-water formation and benthic ecosystems during the past 22 000 years. Quaternary Science Reviews 29, 3006-3020.

Seidel, D.J., Zhang, Y.H., Beljaars, A., Golaz, J.C., Jacobson, A.R., Medeiros, B., 2012. Climatology of the planetary boundary layer over the continental United States and Europe. Journal of Geophysical Research-Atmospheres 117, D17106, doi:10.1029/2012JD018143

Shamir, E., Rimmer, A., Georgakakos, K.P., 2016. The Use of an Orographic Precipitation Model to Assess the Precipitation Spatial Distribution in Lake Kinneret Watershed. Water 8, 591, doi:10.3390/w8120591

Sharifi, A., Pourmand, A., Canuel, E.A., Ferer-Tyler, E., Peterson, L.C., Aichner, B., Feakins, S.J., Daryaee, T., Djamali, M., Naderi Beni, A., Lahijani, H.A.K., Swart, P.K., 2015. Abrupt climate variability since the last deglaciation based on a high-resolution, multi-proxy peat record from NW Iran: The hand that rocked the Cradle of Civilization. Quaternary Science Reviews 123, 215-230.

Sharon, D., and Kutiel, H., 1986. The distribution of rainfall intensity in Israel, its regional and seasonal variations and its climatological evaluation. International Journal of Climatology 6, 277-291.

Stein, M., and Litt, T., 2013. Reply to comment by Christoph Zielhofer and Bernhard Weninger on the article: "Holocene climate variability in the Levant from the Dead Sea pollen record" by Litt et al. Quaternary Science Reviews 49 (2012) 95–105. Quaternary Science Reviews 59, 113-114.

Tarolli, P., Borga, M., Morin, E., and Delrieu, G., 2012. Analysis of flash flood regimes in the North-Western and South-Eastern Mediterranean regions. Natural Hazards Earth System Science 12, 1255-1265.

Theocharis, A., 1989. Deep water formation and circulation in the Aegean Sea. In: Charnock, H. (Ed.), Reports in Meteorology and Oceanography 40, I, pp. 335-359.

Thomas, E.R., Wolff, E.W., Mulvaney, R., Steffensen, J.P., Johnsen, S.J., Arrowsmith, C., White, J.W.C., Vaughn, B., Popp, T., 2007. The 8.2 ka event from Greenland ice cores. Quaternary Science Reviews 26, 70-81.

Timesofisrael. http://www.timesofisrael.com/heavy-downpour-hits-israel-overnight/

Tolika, K., Maheras, P.,Pytharoulis, I., Anagnostopoulou, C., 2014. The anomalous low and high temperatures of 2012 over Greece—An explanation from a meteorological and climatological perspective. Natural Hazards Earth System Science 14, 501–507.

Torfstein, A., Goldstein, S.L., Kagan, E., Stein, M., 2013a. Integrated multi-site U–Th chronology of the last glacial Lake Lisan. Geochimica et Cosmochimica Acta 104, 210-231.

1437 Torfstein, A., Goldstein, S.L., Stein, M., Enzel, Y., 2013b. Impacts of abrupt climate
1438 changes in the Levant from last glacial Dead Sea levels. Quaternary Science Reviews 69,
1439 1-7.

1440 Tubi, A., Dayan, U., 2013. The Siberian High: teleconnections, extremes and association
1441 with the Icelandic Low. International Journal Of Climatology 33, 1357-1366.

1442 Tyrlis, E., Lelieveld, J., Steil., B., 2013. The summer circulation over the eastern
1443 Mediterranean and the Middle East: influence of the South Asian monsoon. Climate
1444 Dynamics 40, 1103-1123.

1445 Tzedakis, P.C., 2007. Seven ambiguities in the Mediterranean palaeoenvironmental
1446 narrative. Quaternary Science Reviews 26, 2042-2066.

1447 Valsecchi, V., Sanchez Goñi, M., Londeix, L., 2012. Vegetation dynamics in the
1448 Northeastern Mediterranean region during the past 23 000 yr: insights from a new
1449 pollen record from the Sea of Marmara. Climate of the Past 8, 1941-1956.

1450 Van Andel, T.H., Runnels, C.N., 1995. The earliest farmers in europe. Antiquity 69, 481-
1451 500.

1452 Vardavas, I.M., Papamastorakis, J., Fountoulakis, A., Manousakis, M., 1997. Water
1453 resources in the desertification-threatened Messara Valley of Crete: estimation of
1454 potential lake evaporation. Ecological Modelling 102, 363-374.

1455 Velaoras, D., Papadopoulos, V.P., Kontoyiannis, H., Papageorgiou, D.K., Pavlidou, A.,
1456 2017. The response of the Aegean Sea (Eastern Mediterranean) to the extreme 2016–
1457 2017 winter. Geophysical Research Letters 44, 9416-9423.

1458 Weatherspark (last visited 1-03-2018).
1459 https://weatherspark.com/averages/32207/Santorini-Thira-South-Aegean-Greece

1460 Weiberg, E., Unkel, I., Kouli, K., Holmgren, K., Avramidis, P., Bonnier, A., Dibble, F., Finné,
1461 M., Izdebski, A., Katrantsiotis, C., Stocker, S.R., Andwinge, M., Baika, K., Boyd, M.,
1462 Heymann, C., 2016: The socio-environmental history of the Peloponnese during the
1463 Holocene: Towards an integrated understanding of the past. Quaternary Science
1464 Reviews 136, 40–65.

1465 Weiss, H., 2000. Beyond the Younger Dryas: collapse as adaptation to abrupt cli¬mate
1466 change in ancient West Asia and the eastern Mediterranean. In G. Bawden and M.
1467 Reycraft (eds), Environmental Disaster and the Archaeology of Human Response.
1468 Anthropological Papers 7. Albuquerque, NM: Maxwell Museum of Anthropology, 75– 98.

1469 Weiss, H. 2017 (ed.). Megadrought and Collapse. From Early Agriculture to Angkor.
1470 Oxford. Oxford University Press.

1471 Weninger, B., Alram-Stern, E., Bauer, E., Clare, L., Danzeglocke, U., Jöris, O., Kubatzki, C.,
1472 Rollefson, G., Todorova, H., van Andel, T, 2006. Climate Forcing Due to the 8200 Cal yr
1473 BP Event Observed at Early Neolithic Sites in the Eastern Mediterranean. Quaternary
1474 research 66, 401-420.

1475 Weninger, B., Clare, L., Gerritsen, F., Horejs, B., Krauß, R., Linstädter, J., Özbal, R., Rohling,
1476 E.J., 2014. Neolithisation of the Aegean and Southeast Europe during the 6600-6000
1477 calBC period of Rapid Climate Change. Documenta Praehistorica XLI, 1-31.

1478 Weninger, B., Clare, L., Rohling, E.J., Bar-Yosef, O., Boehner, U., Budja, M., Bundschuh, M.,
1479 Feurdean, A., Gebel, H.G., Joeris, O., Lindstaedter, J., Mayewski, P., Muehlenbruch, T.,
1480 Reingruber, A., Rollefson, G., Schyle, D., Thissen, L., Todorova, H., Zielhofer, C., 2009. The

1481 impact of rapid climate change on prehistoric societies during the Holocene in the
1482 Eastern Mediterranean. Documenta Praehistorica 36, 7–59.

1483 Weninger, B., Harper, T., The Geographic Corridor for Rapid Climate Change in
1484 Southeast Europe and Ukraine, 2015. In: Svend Hansen, Pál Raczky, Alexandra Anders
1485 and Agathe Reingruber (Eds.), *Neolithic and Copper Age between the Carpathians and the*
1486 *Aegean Sea. Chronologies and Technologies from the 6th to 4th Millennium BC.*
1487 *International Workshop Budapest 2012, Bonn:* Rudolf Habelt, 485-515.

1488 Weninger, B. 2017. Niche Construction and theory of agricultural conditions. Case
1489 studies in punctuated equilibrium. Documenta Praehistorica XLIV, 6-17.

1490 Wittenberg, L., Kutiel, H., Greenbaum, N., Inbar, M., 2007. Short- term changes in the
1491 magnitude, frequency and temporal distribution of floods in the Eastern Mediterranean
1492 region during the last 45 years – Nahal Oren, Mt. Carmel, Israel. Geomorphology 84,
1493 181-191.

1494 WORLD WEATHER NEWS 2001. online: http://www.met.
1495 rdg.ac.uk/~brugge/world2001.html

1496 Xoplaki, E., Maheras, P., Luterbacher, J., 2001. Variability of Climate in Meridional
1497 Balkans during the Periods 1675–1715 and 1780–1830 and its Impact on Human Life.
1498 Climatic Change 48, 581-615.

1499 Yavuz, V., Akçar, N., Schlüchter, C. 2007. The Frozen Bosphorus and its Paleoclimatic
1500 Implications based on a Summary of the Historical Data. In: Yanko-Hombach, V., Gilbert,
1501 A.S., Panin, N., Dolukhanov, P.M. (eds), *The Black Sea Flood Question: Changes in*
1502 *Coastline, Climate, and Human Settlement.* Springer, Dordrecht, 633–649.

1503 Zhang, X., Reed, J., Wagner, B., Francke, A., Levkov, Z., 2014. Lateglacial and Holocene
1504 climate and environmental change in the northeastern Mediterranean region: diatom
1505 evidence from Lake Dojran (Republic of Macedonia/Greece). Quaternary Science
1506 Reviews 103, 51-66.

1507 Zielhofer, C., Weninger, B., 2013. Comment on: "Holocene climate variability in the
1508 Levant from the Dead Sea pollen record" by Litt, T., Ohlman, C., Neumann, F.H., Hense,
1509 A.,. Stein, M., [Quat.Sci.Rev.49 (2012) 95-105]. Quaternary Science Reviews 59, 112.

1510 Zielhofer, C., Clare, L., Rollefson, G., Wächter, S., Hoffmeister, D., Bareth, G., Roettig, C.,
1511 Bullmann, H., Schneider, B., Berke, H., Weninger, B., 2012. The decline of the early
1512 Neolithic population center of 'Ain Ghazal and corresponding earth-surface processes,
1513 Jordan Rift Valley. Quaternary Research 78, 427-441.

1514 Ziv, B., Dayan, U., Kushnir, Y., Roth, C., Enzel, Y., and Ziv, B., 2006. Regional and global
1515 atmospheric patterns governing rainfall in the southern Levant. International Journal of
1516 Climatology 26, 55-73.

1517
1518